Geological Quarterly, 2026, 70, 4
DOI: https://doi.org/10.7306/gq.1849

The accuracy paradox: comparing high-accuracy LiDAR and topographic DEMs for landslide susceptibility assessment in the Slanské vrchy Mountains, Slovakia

Daniel GREGA[1, 3, *], Marián STERCZ[1], Ladislav VIZI[2], Ľubomír PETRO[1], Jaroslav BUŠA[2] and Martin BEDNARIK[3]

[1] State Geological Institute of Dionýz Štúr, Jesenského 8, 040 01 Košice, Slovak Republic; ORCID: 0009-0008-0708-3781 [D.G.]

[2] Technical University Košice, Institute of Geosciences, Faculty of Mining, Ecology, Process Control and Geotechnology, Letná 9, 042 00, Košice, Slovak Republic; ORCID: 0000-0002-5444-0998 [L.V.], 0000-0003-4776-7092 [J.B.]

[3] Comenius University, Faculty of Natural Sciences, Ilkovičova 6, 842 15 Bratislava 4, Slovak Republic; ORCID: 0000-0002-4813-1005 [M.B.]

Grega, D., Stercz, M., Vizi, L., Petro, L., Buša, J., Bednarik, M., 2026. The accuracy paradox: comparing high-accuracy LiDAR and topographic DEMs for landslide susceptibility assessment in the Slanské vrchy Mountains, Slovakia. Geological Quarterly, **70**, 4; https://doi.org/10.7306/gq.1849

The Slanské vrchy Mountains, a volcanic mountain range in eastern Slovakia, is a region critical for engineering-geological research due to the widespread occurrence of diverse forms of slope deformation, conditioned by geological structure, erosion, and gravitational processes, as well as by anthropogenic influences. Given the ongoing research, current attention is focused on applying advanced methods for the registration, investigation, and statistical evaluation of slope deformation structures. In this context, the use of a fifth-generation digital elevation model (DEM 5.0), created using airborne laser scanning (LiDAR), is highly relevant due to its sub-metre accuracy. This model provides an excellent basis for generating parametric maps essential for analysing landslide susceptibility. A critical paradox has emerged: DEM 5.0 captures the terrain after a landslide has occurred, including post-failure features such as steep scarps, which can lead to a misleading interpretation of the original slope conditions. In contrast, older, less precise models, such as DEM 3.5 derived from topographic maps, offer a more suitable representation of the pre-landslide terrain. This is because they better reflect the conditions under which landslides initially formed, avoiding the distortion introduced by post-deformation features. This discrepancy significantly impacts parameters such as slope angle, relief curvature and aspect. This study critically examines this issue by comparing parametric maps derived from DEM 3.5 and DEM 5.0 for the southern Slanské vrchy mountains. While the engineering-geological and land cover maps remain consistent across all three analyses, the DEMs yield differing spatial information for elevation, slope, aspect and curvature. Our findings, validated by receiver operating characteristic (ROC) curves and area under the curve (AUC) values, indicate that analyses using DEM 3.5 consistently yielded a higher predictive accuracy (e.g., AUC of 84.18% for the multivariate model) compared to DEM 5.0 (AUC of 80.89%). This highlights that superior accuracy does not always translate to better suitability for specific geomorphological applications. LiDAR (DEM 5.0) excels at mapping and delineating existing slope deformation structures within GIS, but for generating susceptibility maps, it necessitates removing landslide-affected areas and interpolating the original terrain.

Key words: landslide susceptibility, Slanské vrchy Mountains, DEM resolution, LiDAR, accuracy paradox.

INTRODUCTION

The Slanské vrchy Mountains, a volcanic mountain range in eastern Slovakia, are highly prone to slope failures, making the region a key focus for engineering-geological studies. The region is characterized by diverse slope deformation structuress, such as landslides and block slope failures, which are conditioned by geological structure, erosion, and gravitational processes, as well as by anthropogenic influences. Consequently, these phenomena have a significant negative impact on the environment and the socio-economic sphere, justifying the need for their thorough study.

Landslide susceptibility mapping is a critical tool for geohazard management. It represents the likelihood of a landslide occurring in a specific area based on local terrain conditions (Brabb, 1984; Guzzetti et al., 1999). Susceptibility assessments focus on forecasting the spatial distribution and proneness of the landscape to slope failure (Guzzetti et al., 2005; Pauditš, 2005). Over the past few decades, statistical methods have proven to be a robust approach for this purpose (Carrara, 1983; Chung and Fabbri, 1999).

The territory of Slovakia has a long history of landslide susceptibility assessments employing these methods, with a foundational study by Vlčko et al. (1980) laying the groundwork, followed by a surge in research after 2002 (e.g., Pauditš and

* Corresponding author, e-mail: daniel.grega@geology.sk

Received: October 30, 2025; accepted: February 12, 2026; first published online: March 30, 2026

Bednarik, 2002; Jurko, 2003; Ondrášik et al., 2005; Varga, 2006; Pauditš, 2006; Bednarik, 2007; Krumpálová, 2008; Magulová, 2009; Bednarik and Pauditš, 2010; Grman et al., 2011; Bednarik et al., 2014a). More recently, authors have focused on refining these models by incorporating advanced data sources. For example, Buša et al. (2019) investigated landslide susceptibility in the Košice Basin and the Slanské vrchy using a DEM 3.5, while Tornyai and Koudelka (2024) assessed a region near Čadca with the newer DEM 5.0.

Since 2017, Slovakia has undergone systematic airborne laser scanning (ALS), yielding a fifth-generation digital elevation model (DEM 5.0). This model boasts sub-metre accuracy with a raster resolution of up to 1 1 metre. Its high detail enables the identification of numerous geomorphological features, even in inaccessible areas or beneath dense vegetation. As highlighted by Steger (2020), precise airborne digital elevation models are increasingly used by many researchers as a basis for geomorphological analysis, including the creation of parametric maps for statistical landslide susceptibility assessments. Tools such as ArcGIS Pro and Quantum GIS are commonly used for processing these datasets. The widespread adoption of Airborne Laser Scanning (LiDAR) has revolutionized geomorphological research, providing high-resolution digital elevation models with sub-metre accuracy (Liščák et al., 2022). These highly detailed DEMs are invaluable for identifying subtle geomorphological features, even in inaccessible or densely vegetated areas. Consequently, many studies have utilized high-resolution LiDAR-based data as a primary source for creating parametric maps essential for landslide susceptibility analysis (Tornyai and Koudelka, 2024).

However, the use of high-resolution DEMs for this application is not without its challenges. The scientific community is currently debating whether superior accuracy and detail always lead to improved predictive capability (Ahmed et al., 2025). A number of studies have highlighted a critical paradox: while high-resolution models excel at capturing intricate, real-world features, they may also introduce noise or distortions that are detrimental to susceptibility modelling (Okoli et al., 2023).This is because these models, such as DEM 5.0, accurately represent the terrain in its post-failure state, capturing features like steep landslide scarps and accumulation lobes that are the result of a landslide, not its cause (Guimpier et al., 2022). This can lead to a misinterpretation of the original, pre-landslide slope conditions, skewing the susceptibility analysis and affecting key parameters such as slope angle, curvature, and aspect.

Given these considerations, the primary objective of this paper is to directly compare landslide susceptibility assessments using parametric maps derived from both the older DEM 3.5 and the newer, high-resolution DEM 5.0. While input maps for lithology and land cover are identical, the core difference lies in the maps for elevation, slope, aspect, and relief curvature which are derived from the two distinct DEMs. Our findings, verified using ROC curves and AUC values, demonstrate that the analysis using the older DEM 3.5 yielded a higher predictive accuracy. This finding challenges the conventional assumption that a higher resolution is always superior for susceptibility modelling. Instead, it suggests that for LiDAR data to be effectively used for this purpose, a significant pre-processing step may be required to remove existing landslide features and interpolate the terrain before the landslide was triggered.

GEOLOGICAL SETTING

The central point of the area is the stratovolcano Veľký Milič, which has an elevation of 893.5 m a.s.l. This locality, situated southeast of Košice city, is defined by the cadastral territories of 17 municipalities in the Košice Region (Fig. 1).

Most of these municipalities have experienced intense manifestations of slope deformation in the recent past. The year 2010 is characterized in the context of Slovakia as the “year of landslides” (Grman et al., 2010; Liščák et al., 2010), when, after heavy rainfall, many examples of slope deformation originated or were reactivated, especially in eastern Slovakia, including our study area. The affected municipalities include, for example, Nižná Myšľa, Vyšný Čaj, Slanec and Nižná Hutka. The southern boundary of the area is formed by the state border with Hungary. The total area of the territory studied is 189.6 km^2.

From a geomorphological perspective, the area evaluated is situated in the southern part of the Slanské vrchy mountain range and belongs to the Alpine-Himalayan system, the Carpathian subsystem, the Western Carpathian province, the Inner Western Carpathian sub-province, and the Matra-Slanec Area. Part of the Košická kotlina (Košice Basin) also falls within the extent of the territory (Mazúr and Lukniš, 1978).

From a geological perspective, the Slanské vrchy is part of the East Slovak Neogene Volcanics belt, which lies on older Neogene strata. Their formation dates back to the Badenian to Pannonian ages. Currently, they represent an eroded remnant of extensive original volcanic structures (Kaličiak and Žec, 1995). In addition to Neogene strata, Quaternary deposits are also found in the area, specifically those of slope (deluvial), proluvial, eolian, and fluvial origin (Kaličiak et al., 1996).

Landslides represent the dominant type of slope deformation structures in the study area. These failures predominantly developed in the peripheral parts of the mountain range, specifically in contact zones with Neogene strata. Here, their formation is conditioned by the lithological interface between the impermeable volcanic rocks and the overlying, less competent Neogene clay strata. This interface often leads to the concentration of groundwater and high pore water pressure, severely reducing slope stability. Within the central volcanic structures, landslides are present in deep valleys sculpted by erosion. Additionally, block slides, block fields, scree slopes and boulder fields are present in the study area (Nemčok, 1982).

MATERIALS AND METHODS

DIGITAL ELEVATION MODELS IN SLOVAKIA, PARAMETRIC MAPS AND INPUT DATA

Digital Elevation Model 3.5 (DEM 3.5) represents the Earth’s surface devoid of objects, consisting of a point set with defined spacing that contains coordinate and elevation data. Fundamentally based on DEM 3, which was developed through the vectorization of topographic maps (primarily at 1:10,000 scale, supplemented by 1:25,000), DEM 3.5 was originally created to generate contour lines for cartographic representation, with certain areas also enhanced using elevation data from the Basic Map of the Slovak Republic 1:10,000 (ZM SR 1:10,000) series. The Military Topographic Institute of the Slovak Army historically generated gridded data from these sources at resolutions such as 10 10 to 100 100m; however, for our specific purposes, we utilized the vectorized contour lines at 2 m intervals, from which a raster was subsequently created with a cell size of 1x1 m. Furthermore, DEM 3.5 corrects errors present in the original DEM 3, such as incorrectly entered contour line elevations, by correcting erroneous points through deletion and subsequent remolding using surrounding data, contour lines from the 1:10,000 Basic Map, or data from DEM 4.

In the Slovak Republic, the full-scale use of airborne laser scanning began in 2017. During this period, the Geodesy, Cartography and Cadastre Authority of the Slovak Republic (GCCA SR) started systematic scanning of the entire state territory, which was completed in May 2023. Scanning was generally

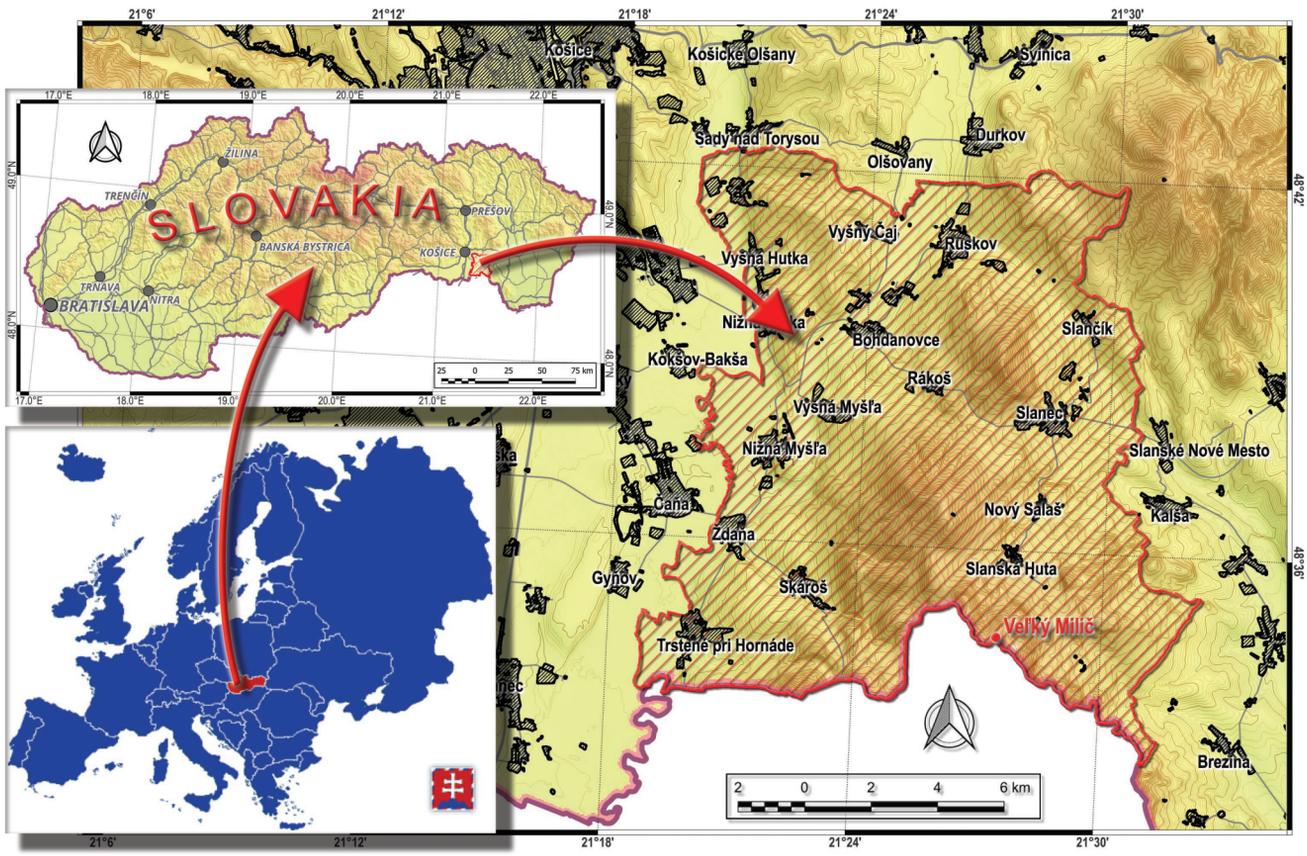

Fig. 1. Map of study area (processed in QGIS, data based on GCCA SR ortophoto map)

performed during the non-vegetation period, from November to April of the following year. Planning also required consideration of meteorological conditions such as precipitation, fog, and especially snow cover.

The primary output of the scanning process is a point cloud, which, after post-processing, is used to derive either a Digital Surface Model (DSM) or a Digital Elevation Model (DEM). The DEM 5.0 is generated as a raster (GRID) with a 1x1 m resolution. This model is interpolated from the classified points assigned to the "ground" class within the point cloud. The interpolation method used is the Inverse Distance Weighting (IDW) algorithm, employing an exponent of 2 and a maximum of 12 neighboring points. The accuracy of the DEM 5.0 is high, with a reported horizontal accuracy of 0.03 m and a vertical accuracy of 0.09 m (Leitmanová and Gálová, 2023). Most suppliers are also capable of detailed classification of the point cloud, which allows for the simultaneous generation of the DSM 1.0. This model is likewise generated in GRID format with a 1 1 m resolution and interpolated from selected point cloud classes (specifically excluding "low point (noise)" and "high point (noise)"), using the same IDW algorithm as for the DEM 5.0.

The statistical analysis itself was preceded by the creation of parametric maps. For our purposes, we selected the following seven parameters that influence slope stability:

- map of registred landslides,
- reclassified thematic engineering-geological map,
- land cover map,
- elevation map,
- aspect map,
- slope gradient map,
- curvature map.

All data were processed in the QGIS software environment with a raster resolution of 1 1 metre. For the purpose of landslide susceptibility assessment, three input maps were kept consistent across all three analyses: a map of registred landslides, a reclassified thematic engineering-geological map and a land cover map. The crucial difference lies in the derivation of the remaining four parametric maps: elevation, slope orientation (aspect), slope gradient, and relief curvature. These maps were generated independently of both DEM 3.5 and DEM 5.0, allowing for a direct comparison of their influence on the resulting susceptibility models.

The first parameter evaluated is the map of registered landslides. The inventory for the susceptibility analysis utilizes 364 identified landslides. We focus exclusively on this type of movement, as other slope deformation structures (e.g., block slides) represent different mechanisms and stability factors, making them unsuitable for the current statistical model. The activity states of these landslides are categorized according to the regional classification of Nemčok (1982; Table 1) into three main categories (Fig. 2):

- active (14.44%): currently moving or recently moved;
- dormant/potential (67.34%): temporarily stable, but capable of renewed movement under critical conditions (e.g., heavy rainfall or earthquake);
- stabilized (18.22%): movements have ceased, typically due to long-term natural changes or human intervention, making them currently safe.

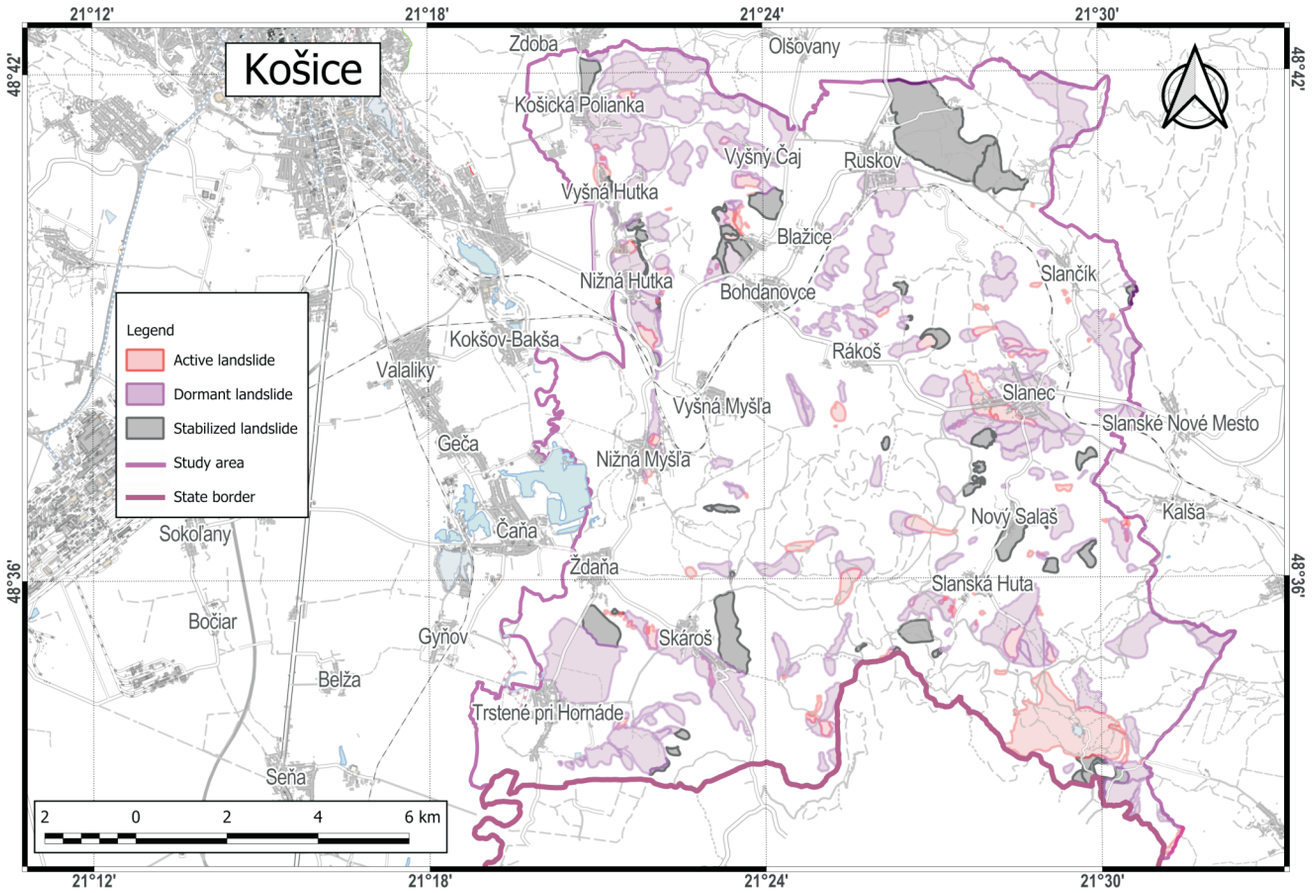

Fig. 2. Landslide map of study area (data based on Liščák et al., 2018)

Table 1

Distribution of landslide classes within the entire study area (km² and %)

Activity	Number of landslides	Area [km²]	Area [%]	Area total [%]
Active	114	6.38	14.44	3.37
Dormant	191	29.75	67.34	15.69
Stabilized	59	8.05	18.22	4.25
SUM	364	44.19	100.00	23.30

For international comparability, the movement types are cross-referenced with the globally accepted classifications of Varnes (1978) and Hungr et al. (2014). Landslides together account for 23.30% of the total study area.

The landslide map itself was compiled based on the project "Identification, Registration, and Engineering-Geological Mapping of Slope Deformations" (Liščák et al., 2018). This project included the actual field mapping of slope deformation structures, with their boundaries subsequently refined using DEM 5.0 data. The landslide boundaries are thus delineated with sub-metre accuracy, ensuring a high-quality, up-to-date inventory for the susceptibility analysis.

The second parametric map is the reclassified engineering-geological map, derived from the original 1:10,000 scale mapping produced during the project "Identification, Registration, and Engineering-Geological Mapping of Slope Deformations" (Liščák et al., 2018). The lithology of the study area was reclassified into six fundamental classes. Neovolcanic rocks form the bedrock of the area, represented by various types of andesite lavas and their volcanoclastic equivalents. The sedimentary cover is dominated by Quaternary slope (deluvial) (loamy-stony and debris-clay deposits) and fluvial deposits (gravels, sands and silts). The Neogene strata, which are critical for slope stability, belong primarily to the Stretava Formation (Košice gravels) and consist of a heterogeneous mixture of gravels, clays, sands and tuffaceous horizons. Aeolian (loess and loess-clays) and proluvial deposits (alluvial fans) represent a smaller portion of the territory (Table 2). A significant advantage of this map is that DEM 5.0 visualizations, specifically shaded relief and positive openness methods, were employed to refine the mapped lithological boundaries with high precision (Fig. 3A).

The third parameter analysed is the land cover map. The primary data source was the vector map (GCCA SR, 2024) derived from the ZB GIS catalogue (Geodetic and Cartographic Institute Bratislava), which was subsequently reclassified into eight categories. The territory is dominated by forest stands, consisting mainly of deciduous and mixed forests typical of the Slanské vrchy Mts., and arable land, which prevails in the lower-lying basins. Other categories include shrubland (representing transitional woodland-shrub stages), gardens, and

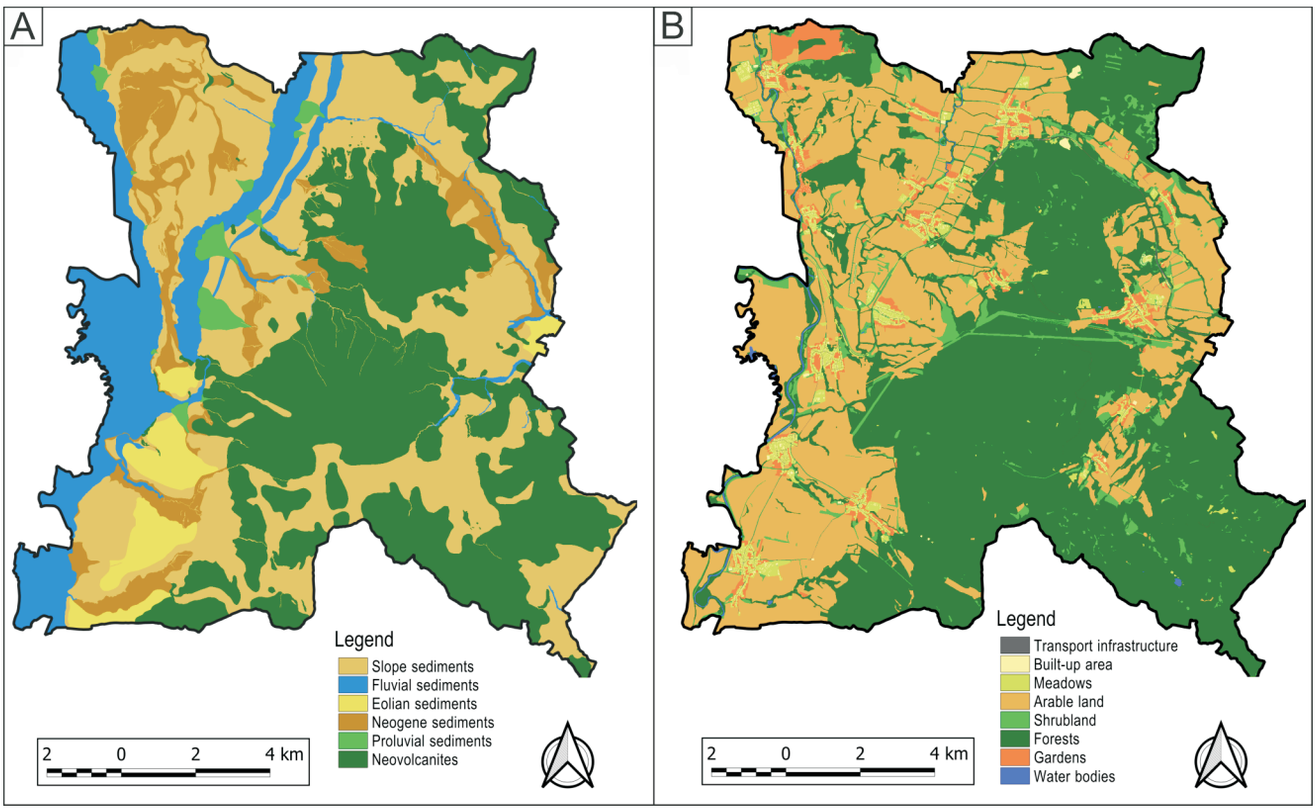

Fig. 3A – reclassified thematic engineering-geological map (data based on Liščák et al., 2018); B – landcover map (data based on ZB GIS catalogue)

Table 2

Distribution of engineering-geological classes within the entire study area (km^2 and %)

Class	Genetical type	Area [km²]	Area [%]
1	Slope deposits	67.69	35.70
2	Fluvial deposits	25.59	13.50
3	Aeolian deposits	7.29	3.84
4	Neogene strata	16.20	8.54
5	Proluvial deposits	2.86	1.51
6	Neovolcanic rocks	69.98	36.91

Table 3

Distribution of land cover classes within the entire study area (km^2 and %)

Class	Description	Area [km²]	Area [%]
1	Transport infrastructure	0.96	0.51
2	Built-up area	1.63	0.86
3	Meadows	6.22	3.28
4	Arable land	67.58	35.64
5	Shrubland	8.69	4.58
6	Forests	98.00	51.69
7	Gardens	5.64	2.98
8	Water bodies	0.88	0.46

meadows (permanent grasslands). Human-impacted areas are represented by built-up areas and transport infrastructure, while the smallest portion of the territory consists of water bodies (Fig. 3B). The detailed percentage representation of each category is provided in Table 3.

The fourth parameter is the elevation map, derived from both DEM 5.0 (Fig. 4A) and DEM 3.5 (Fig. 4B). The model was reclassified into 8 classes using a uniform 100-metre vertical interval. This classification was chosen over the traditional geomorphological belts of Slovakia (Mazúr and Lukniš, 1978) to achieve a more balanced and statistically robust distribution of data across the classes.

The starting threshold for the elevation intervals was set at 212 m a.s.l. This specific value was adopted to maintain methodological continuity with previous landslide susceptibility research in the Slanské vrchy Mts. (e.g., Buša et al., 2019). By preserving these specific interval boundaries, we ensured that the new models derived from both DEM 3.5 and DEM 5.0 remain directly comparable with existing regional datasets and previous statistical evaluations.

For both digital elevation models, the distribution of classes is nearly identical. The most significant portion of the territory is situated within the 212–312 m a.s.l. range. Detailed area representation and percentage shares for all elevation classes are summarized in Table 4.

The aspect map is a crucial parameter, as it significantly influences the microclimatic conditions of the slopes. Slope orientation affects the intensity of solar radiation, which directly impacts evapotranspiration rates and soil moisture retention (Pauditš, 2005). Furthermore, slope aspect plays a role in the spatial distribution of precipitation. In the Western Carpathians, including the Slanské vrchy Mts., prevailing winds from the west and north-west often create a rain-shadow effect. The wind-

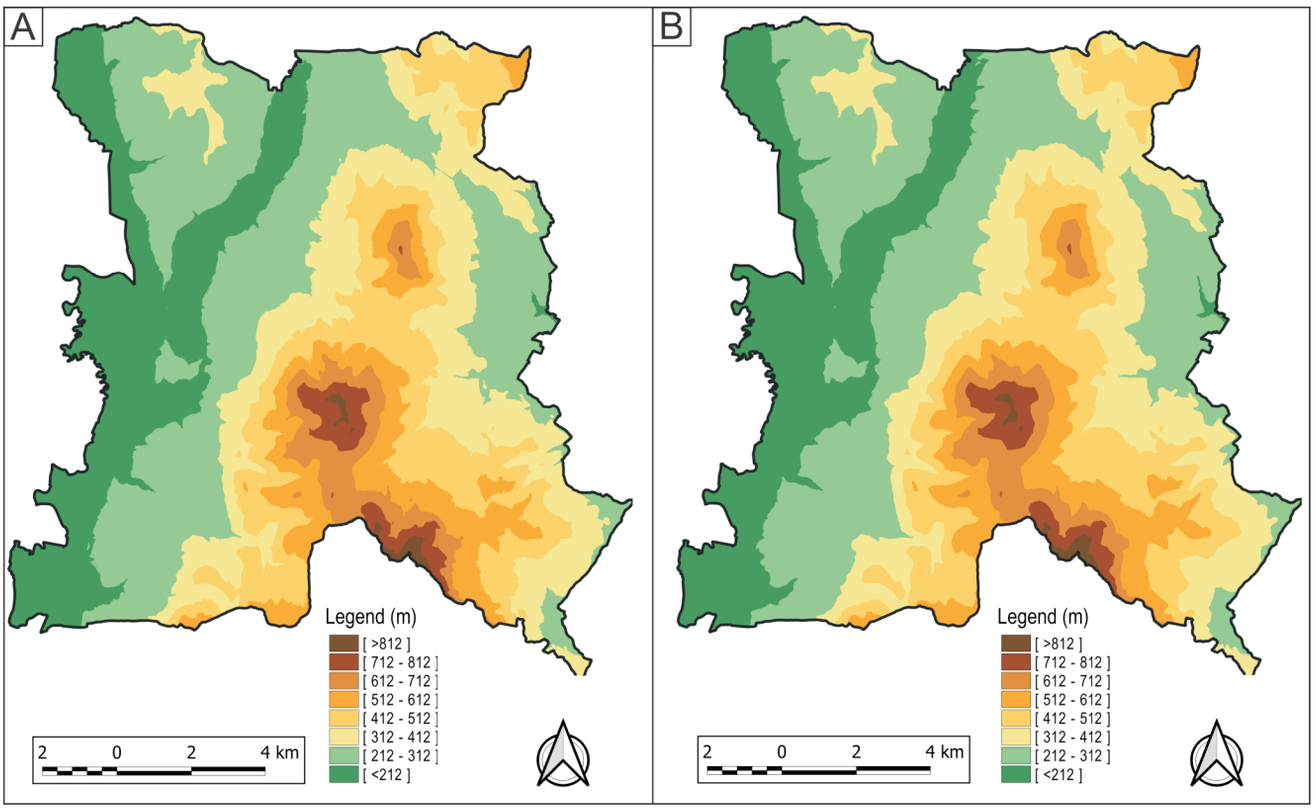

Fig. 4A – reclassified elevation map of the study area processed in QGIS using DEM 5.0 data; B – DEM 3.5 data

Table 4

Distribution of elevation classes within the entire study area based on DEM 5.0 and DEM 3.5 (km^2 and %)

Class	Interval [m a.s.l.]	Area DEM 5.0 [km^2]	Area DEM 5.0 [%]	Area DEM 3.5 [km^2]	Area DEM 3.5 [%]
1	(<212)	34.51	18.20	34.80	18.35
2	(212–312)	60.14	31.72	59.97	31.63
3	(312–412)	38.06	20.07	37.94	20.01
4	(412–512)	29.01	15.30	28.90	15.24
5	(512–612)	15.86	8.36	15.80	8.33
6	(612–712)	7.57	3.99	7.72	4.07
7	(712–812)	3.70	1.95	3.70	1.95
8	(>812)	0.76	0.40	0.78	0.41

ward slopes (W, NW) are typically exposed to higher cumulative rainfall and more frequent intense precipitation events, which can lead to increased pore water pressure and the subsequent triggering of landslides.

This parameter was reclassified into nine classes: the eight cardinal directions and flat terrain. The distribution of slopes based on aspect varies slightly between the two models. In both DEM 5.0 (Fig. 5A) and DEM 3.5 (Fig 5B), west-facing slopes dominate the study area, while south-facing slopes and flat terrain have the smallest representation. The comprehensive statistical distribution of aspect classes for both models is summarized in Table 5.

Slope gradient is a fundamental factor in slope stability analysis as it directly determines the components of gravitational force. An increase in the slope angle leads to higher shear stress acting along the failure surface. In our assessment, this parameter was integrated as a continuous variable reclassified into nine classes according to Matula et al. (1983), allowing for the identification of critical threshold angles.

The analysis reveals that the majority of the study area (~65%) is characterized by slopes ranging from 3 to 17°. Within this range, the most frequent inclinations are between 7 and 11°, which correspond to the typical geomorphological setting of the landslide-prone peripheral zones of the Slanské vrchy Mts. A significant finding is the discrepancy in steeper terrain representation; the high-resolution DEM 5.0 captures a much larger portion of slopes above 31° (1.95%; Fig. 6A) compared to the older DEM 3.5 (0.15%; Fig. 6B), which heavily generalizes extreme relief features. All detailed values are summarized in Table 6.

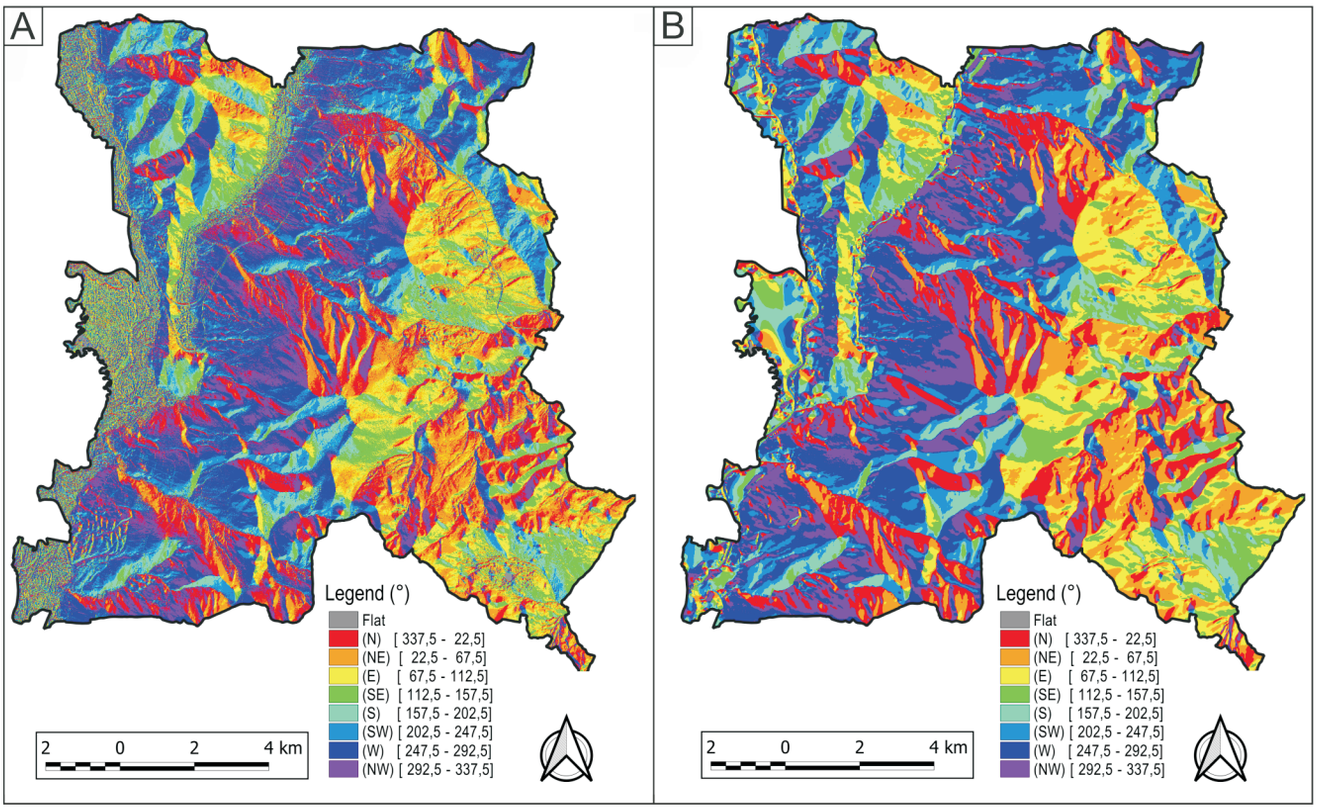

Fig. 5A – reclassified aspect map of the study area processed in QGIS using DEM 5.0 data; B – DEM 3.5 data

Table 5

Distribution of slope aspect classes within the entire study area based on DEM 5.0 and DEM 3.5 (km² and %)

Class	Interval [°]	Area DEM 5.0 [km²]	Area DEM 5.0 [%]	Area DEM 3.5 [km²]	Area DEM 3.5 [%]
1	flat (–1)	0.25	0.13	0.11	0.06
2	N (337.5–22.5)	22.98	12.12	21.76	11.47
3	NE (22.5–67.5)	24.28	12.81	24.35	12.84
4	E (67.5–112.5)	22.46	11.84	21.89	11.54
5	SE (112.5–157.5)	17.42	9.19	17.97	9.48
6	S (157.5–202.5)	16.58	8.75	16.28	8.58
7	SW (202.5–247.5)	23.13	12.20	22.02	11.61
8	W (247.5–292.5)	34.03	17.95	35.49	18.72
9	NW (292.5–337.5)	28.48	15.02	29.75	15.69

Slope curvature is a critical parameter for assessing surface processes, as it controls the acceleration and convergence of water runoff and material transport. Profile curvature affects the flow velocity, while planform curvature influences the spatial concentration of surface water (Mitasova et al., 1995). In this study, we distinguish three primary geomorphological forms: convex, concave, and linear.

A crucial methodological step was defining the interval for linear (planar) forms. Based on the regional characteristics and to maintain consistency with previous susceptibility research in the Slanské vrchy Mts. (e.g., Buša, 2019), we adopted the threshold values from Tornyai and Dunčko (2013), ranging from -0.00025 m^{-1} to 0.00025 m^{-1}.

The results reveal a fundamental discrepancy between the two models. The high-resolution DEM 5.0 is almost evenly divided between convex and concave forms, with linear forms representing only a negligible portion of the area. This distribution highlights the LiDAR model's ability to capture micro-relief complexity, although at certain scales it may appear as a "complex overlay" of overlapping features (Fig. 7A). In contrast, the DEM 3.5 is dominated by linear forms, which is a direct consequence of the smoothing effect and lower resolution of the source data, leading to a more generalized representation of the terrain (Fig. 7B). Detailed quantitative data for all curvature classes are summarized in Table 7.

FREQUENCY RATIO

The Frequency Ratio (*FR*) method is a quantitative statistical approach widely used for landslide susceptibility mapping. Its popularity stems from its straightforward calculations and easy-to-interpret results, making it an ideal choice for GIS-ba-

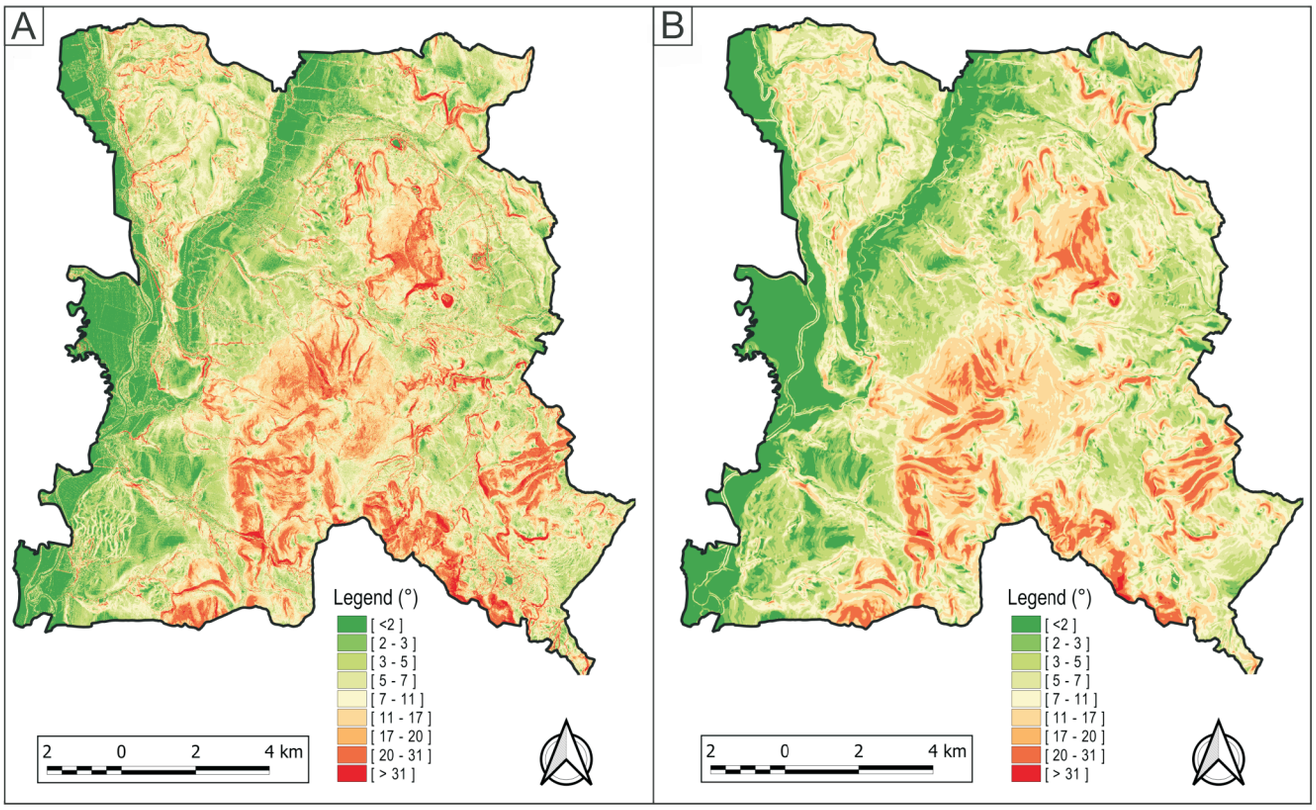

Fig. 6A – reclassified slope gradient map of the study area processed in QGIS using DEM 5.0 data; B – DEM 3.5 data

Table 6

Distribution of slope gradient classes within the entire study area based on DEM 5.0 and DEM 3.5 (km² and %)

Class	Interval [°]	Area DEM 5.0 [km²]	Area DEM 5.0 [%]	Area DEM 3.5 [km²]	Area DEM 3.5 [%]
1	(<2)	24.40	12.87	24.43	12.89
2	(2–3)	13.51	7.13	11.96	6.31
3	(3–5)	31.10	16.40	32.17	16.97
4	(5–7)	29.19	15.39	34.02	17.95
5	(7–11)	35.37	18.66	39.70	20.94
6	(11–17)	27.22	14.36	28.79	15.19
7	(17–20)	8.75	4.61	8.62	4.55
8	(20–31)	16.37	8.63	9.58	5.05
9	(>31)	3.69	1.95	0.29	0.15

sed analysis. The core principle of the method is to quantify the spatial relationship between landslide occurrences and individual environmental factors. The resulting *FR* values serve as weights for each class of a given parameter, reflecting its relative importance in landslide formation (Gulbet and Getahun, 2024).

The key step in the *FR* method is calculating the frequency ratio for each discrete class (category) within a given parameter (e.g., lithology, slope or aspect). The *FR* value is obtained by comparing two ratios:

- the ratio of the area of landslides within a given class to the total landslide area in the study region;
- the ratio of the total area of that class to the total area of the entire study region.

Mathematically, this principle is expressed by the following formula:

$$FR \quad \frac{A_{cl} / A_l}{A_c / A} \qquad [1]$$

where: A_{cl} – the area of a parameter's class that is affected by a landslide; A_l – the total landslide area in the entire study region; A_c – the total area of the given parameter's class; A – the total area of the entire study region.

The resulting *FR* values can be interpreted as follows:

- $FR > 1$ – this value indicates that the given class is highly susceptible to landslides, as they occur more frequently within this class than would be expected.
- $FR < 1$ – this value suggests low susceptibility.
- $FR = 1$ – this value indicates average susceptibility, meaning landslides occur within this class at a rate similar to that of the entire study area.

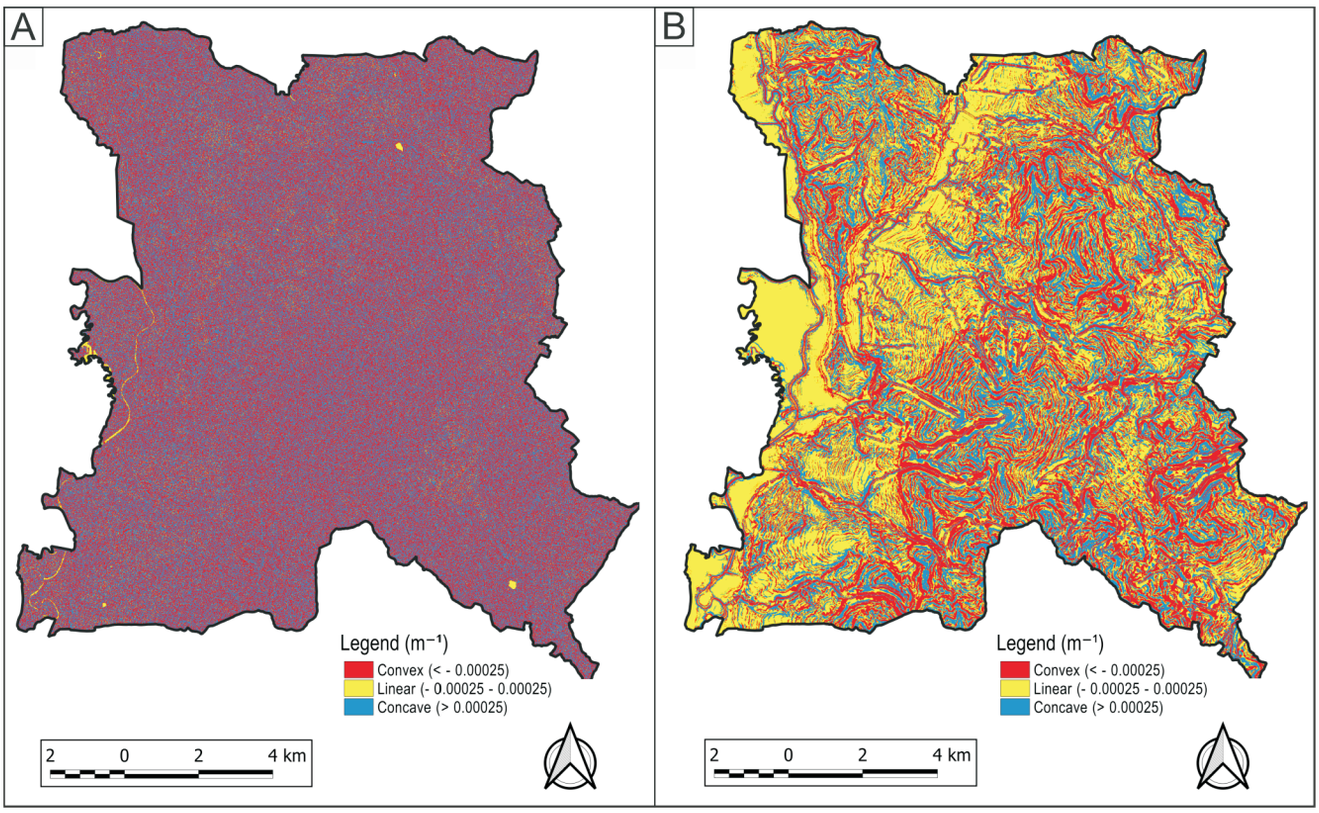

Fig. 7A – reclassified curvature map of the study area processed in QGIS using DEM 5.0 data; B – DEM 3.5 data

Table 7

Distribution of curvature classes within the entire study area based on DEM 5.0 and DEM 3.5 (km² and %)

Class	Interval [m⁻¹]	Area DEM 5.0 [km²]	Area DEM 5.0 [%]	Area DEM 3.5 [km²]	Area DEM 3.5 [%]
1	convex (< –0.00025)	93.27	49.19	62.32	32.87
2	linear (–0.00025–0.00025)	4.29	2.26	70.93	37.41
3	concave (>0.00025)	92.04	48.54	56.36	29.72

After calculating the *FR* values for all classes of each parameter, the original raster layers are reclassified. The initial class values are replaced with the calculated *FR* values. This step is crucial because it transforms qualitative or quantitative environmental data into weights that express their significance in landslide formation.

The next step is to create the final susceptibility map by summing all the reclassified raster layers. The resulting map, where each pixel holds the cumulative sum of the *FR* values from all influencing parameters, represents a cumulative landslide susceptibility index. Areas with a high sum of FR values are identified as zones of high susceptibility, while those with a low sum are considered stable.

BIVARIATE ANALYSIS

Bivariate statistical analysis of the landslide susceptibility is based on the comparison of a landslides occurrence and a set of the input factors that affect the stability slopes. As mentioned before, all input factors are prepared in form of a raster (or a grid) as a set of parametrical maps (or index maps; Pauditš et al., 2014, or thematic data layers; Pourghasemi et al., 2012) with the same geometrical properties: grid origin, grid resolution and area selection studied. The raster resolution for each parametrical map is 1 1 m (1 m^2), with total number of cells within the area under study after geographic selection equal to 189 609 740 (m^2).

The landslide parametrical map represents a spatial dichotomous variable with only two possibilities, such as a presence or absence of landslide cell within the study area. These two possibilities form a mutually exclusive and exhaustive system of the events, since the two events cannot happen at the same time. They also refer to disjoint events where the probability between them will have a zero value – there is no probability for them to occur simultaneously; or their intersection is an empty set; or these two events have no outcomes in common:

$$P\ 1\ \ 0 \quad P\ 0\ \ 1\ \ 0 \qquad [2]$$

The notion “exhaustive” refers that an event (one of them) must occur. Let us denote by *A* the study area, discriminated into a total *N*(*A*) number of cells (189 609 740 in our case). The code “1” will represent a raster cell with the presence of a landslide (positive cells) and code “0” is its complement such as:

$$N(1) \quad N(0) \quad N(A) \qquad [3]$$

In the other words, the sum of number cells with landslide and without landslide is equal to the total number of cells within the study area. Since the presence or absence of landslides within the study area form an exhaustive system of events, their respective probabilities P will sum up to 1:

$$\frac{N(1)}{N(A)} \quad \frac{N(0)}{N(A)} \quad P(1) \quad P(0) \quad 1 \qquad [4]$$

Let us consider an individual factor as "F". As noted above, we have a set of the individual input factors F_i; i = 1, …, n; in form of the parametrical or index maps. We will use the letter "F" instead of "P" for the parametrical map, so as not to create confusion with a probability notation.

Now, we assume that F_i is originally categorized into m classes of discrete indices; j = 1, …, m_i; (for instance geology or landcover) or has continuous factor values and these are subdivided into m_i discrete index classes (for instance slope or aspect). The process is known in the GIS community as a (primary) reclassification. From the point of view of probability theory, the m classes of a factor i represent a set of outcomes with a set of distinct possibilities that exhaust the possible results. By definition, given a finite set of outcomes, the probability of each outcome is a number between 0 and 1, assigned in such a way that the sum of the probabilities of all outcomes is equal to 1 – neither more nor less.

The total number of cells for the m classes of the ith factor within layer F_i is equal to $N(A)$:

$$\sum_{j\ 1}^{m_i} N\ F_{i,j} \qquad N(F_i) \quad N(A) \text{ for } i = 1,\ldots, n;\ j = 1,\ldots, m_i \qquad [5]$$

Analogously to the landslide parametric map, a set of m_i classes of a factor F_i form a mutually exclusive and exhaustive system of events, and summation of their individual probability of occurrence is equal to one (their intersection is an empty set):

$$\sum_{j\ 1}^{m_i} \frac{N(F_{i,j})}{N(A)} \quad \sum_{j\ 1}^{m_i} P_{i,j} \quad 1 \qquad [6]$$

Each factor map F_i is overlapped with the landslide inventory map to obtain a number of landslide pixels for each individual class j of the factor map – hence the bivariate analysis.

Many bivariate methods have been proposed and applied in landslide susceptibility analysis. An excellent review can be found in Li and Lan (2023). In this article, we followed the methodology proposed by Vlčko et al. (1980), known as the entropy index or index of entropy (Li and Lan, 2023).

The method proposed is based on a process of weighting of an information coefficient, which is obtained from the standardised difference of a factor entropy and its maximum entropy. The methodology workflow starts with calculation of the relative frequencies of the positive landslide cells within the jth class of factor F_i, $1_{i,j}$, to the total cells of the jth class of factor F_i, $F_{i,j}$:

$$R_{i,j} \quad \frac{N(1_{i,j})}{N(F_{i,j})} \qquad [7]$$

The ratio is, in Vlčko et al. (1980), denoted as the "probability" of landslide occurrence for each class jth of factor F_i, $F_{i,j}$. We denote those relative frequencies as "R" instead of "P", which will be reserved for probability in the following text.

The next step is to normalise every relative frequency $R_{i,j}$ relative to the sum of all probabilities to get the "probability density" (Vlčko et al., 1980):

$$P_{i,j} \quad \frac{R_{i,j}}{\sum_{j\ 1}^{m} R_{i,j}} \qquad [8]$$

It has been claimed (Li and Lan, 2023) that the ratio represents the conditional probability of landslide presence, given as $F_{i,j}$. The conditional probability is equal to the ratio of landslide pixels' intersections with the jth class of factor F_i:

$$R_{i,j} \quad \frac{N\ 1\ \ F_{i,j}}{N(F_{i,j})} \quad \frac{P\ 1\ \ F_{i,j}}{P(F_{i,j})} \quad P\ 1|F_{i,j} \qquad [9]$$

Unfortunately, the summation of the conditional probabilities $P(1|F_{i,j})$ for all classes of a given factor is not equal to 1 (the universal condition). Only the conditional probabilities of landslide appearance given $F_{i,j}$ and landslide absence given $F_{i,j}$ sum up to 1 because, as stated before, the "presence" and "absence" of a landslide are mutually exclusive and exhaust a subarea $F_{i,j}$. This means the summation of all conditional probability for each of the classes j = 1, …, m_i of any factor F_i leads exactly to the number of classes m of the factor F_i. In other words, the landslide presence itself does not constitute an exhaustive system of the events without its complement. The conditional probability $P(1|F_{i,j})$ indicates that we are considering the probability of landslide presence relative to the factor class $F_{i,j}$.

Let us take a deeper look at "probability density". The probability can be expressed as follows:

$$P_{i,j} \quad \frac{N\ 1\ \ F_{i,j}\ /N(F_{i.j})}{\sum_{j\ 1}^{m} N\ 1\ \ F_{i,j}\ /N(F_{i,j})} \quad \frac{P\ 1|F_{i,j}}{\sum_{j\ 1}^{m} P\ 1|F_{i,j}} \qquad [10]$$

The equation can be written in form of a conditional probability:

$$P_{i,j} \quad \frac{N\ 1_{i,j}\ \ F_{i,j}\ /N(A)}{N(1)/\ N(A)} \quad \frac{P\ 1\ \ F_{i,j}}{P(1)} \quad P\ F_{i,j}|1 \qquad [11]$$

This time, the conditional probabilities $P(1|F_{i,j})$ sum up to 1. Since in practice we are not interested in subareas without landslide occurrences, the set of classes j of factor i, $F_{i,j}$, within the landslide subareas constitutes a mutually exclusive and exhaustive system of the events. In fact, if we consider that $P(1)$ 0, then the roles of $F_{i,j}$ and 1 are interchangeable because $F_{i,j}$ 1 is the same as 1 $F_{i,j}$ and it follows that:

$$P\ 1\ \ F_{i,j} \qquad P(1)P\ F_{i,j}|1 \ \textit{or}\ P\ F_{i,j}|1 \quad \frac{P\ 1\ \ F_{i,j}}{P(1)} \qquad [12]$$

The classes m of mutually exclusive events constitutes a set of random outcomes of a respective factor i, which is considered as a random variable. Given a set of the probabilities of the occurrence of m_i classes within the landslide subareas, the **entropy** of a random variable can be written as:

$$H_i \quad \sum_{j\ 1}^{m_i} P_{i,j} \log_2 P_{i,j} \quad or\ H_i \quad \sum_{j\ 1}^{m_i} P_{i,j} \log_2 \frac{1}{P_{i,j}} \qquad [13]$$

where $-\log_2(P_{i,j})$, or $\log_2(1/P_{i,j})$, is the **information content** C_i of a random event F_i, which is a function increasing in an indirect way as the probability of $P_{i,j}$ decreases.

The entropy in terms of the information content expresses the expected amount of information transferred by identifying the possible outcomes of a random trial:

$$H \quad E[C_i] \quad E \quad \log_2(P_{i,j}) \qquad [14]$$

where E is the expected value operator. The expected value is calculated as a linear combination (weighted average), where the weights for each information content C_i is given by the respective probability $P_{i,j}$ with respect to the universal condition that the sum of the probabilities is one. From the above, the entropy of a random variable quantifies the average level of uncertainty associated with the variable's possible outcomes.

The final entropy of a factor F_i is compared to its maximal entropy. Under the universal condition that the sum of probabilities equals to one, the maximum entropy discrete probability distribution among m mutually exclusive events is the uniform distribution:

$$P_{i,j} \quad \frac{1}{m_i} \quad \text{for} \quad j = 1, \ldots, m_i \qquad [15]$$

The expression states that the least informative distribution would occur when there is no reason to favour any one of the class j over the others. In that case, each class has the same probability to occur, which leads to the uniformity of the probability distribution – nothing is more probable than the other. Then, the entropy would be equal to its maximum possible value, which is given as:

$$H_{\max} \quad \sum_{j\ 1}^{m_i} P_{i,j} \log_2 P_{i,j} \quad \sum_{j\ 1}^{m_i} \frac{1}{m_i} \log_2 \frac{1}{m_i} \quad \log_2(m_i) \qquad [16]$$

The entropy can be therefore be seen as a numerical measure, which describes how uninformative a particular probability distribution is. It ranges from zero for total classes of factor F_i ($m_i = 1$) as completely informative, to $\log_2(m_i)$, which results in a completely uninformative situation. When the entropy is zero, it is a case of impossibility with probability $P_{i,j} = 0$ for all or $m_i - 1$ classes j, or total certainty with probability $P_{i,j} = 1$ for one class j. In these cases, there is no uncertainty at all; simply because there is no choice.

The standardised difference between the maximal entropy and entropy defines the information coefficient I_i:

$$I_i \quad \frac{H_{\max_i} \quad H_i}{H_{\max_i}} \quad 1 \quad \frac{H_i}{H_{\max_i}} \qquad [17]$$

The information coefficient ranges from 0 to 1, depending on how close is the entropy of a factor F_i to its maximal entropy.

Bivariate statistical analysis of the landslide susceptibility results in an continuous output variable, spatially distributed on an input grid covering a study area. The output variable is obtained as a linear combination of the secondary reclassified indices and the weights for each input factor. The secondary reclassification is based on the calculated probability score, where a class with no occurrence within the landslide gets the index equal to zero and the class with the highest probability gets the value equal to the topmost index of the primary reclassification and so on. The respective weights w_i for the input factor F_i are calculated as the product of the information coefficient I_i and the average probability:

$$w_i \quad I_i \ \overline{P_{i,j}} \qquad [18]$$

To ensure unbiased estimation of the landslide sustainability values, the weights obtained were normalised to respect the universal condition that the weights sum up to 1:

$$\sum_{i\ 1}^{n} w_i \quad 1 \qquad [19]$$

The final linear combination of the landslide sustainability values LSS is calculated in the form of a weighted average as a product of the calculated weights w_i and the secondary reclassified classes of factor:

$$LSS \quad \sum_{i\ 1}^{n} F_{i_2} \ w_i \qquad [20]$$

MULTIVARIATE ANALYSIS

Multivariate statistical analysis represents an advanced method applied in landslide susceptibility assessment, which involves the combination of all input data layers (Bednarik et al., 2014b). Unlike bivariate statistical analysis, this approach does not incorporate a weighting process for individual parameters during the susceptibility evaluation (Holec et al., 2018).

In the case of conditional analysis, the mutual combination of input parametric maps results in a table containing all possible combinations of categories across all input maps. The outcomes of these combinations are new spatial units referred to as Unique Conditional Units (UCUs). These are formed by the spatial overlaying of individual categories from the parametric maps onto each other and represent a quasi-homogeneous unit (Pauditš, 2005).

Landslides located within the resulting combinations (areas with landslides are assigned a value of 1, areas without landslides a value of 0) are then ranked based on their calculated intensity of occurrence. This intensity is expressed as the ratio of the number of UCU cells with landslides to the total area of the UCU, and the results are subsequently ordered in descending order for the individual combinations, acquiring values ranging from 0 to 100%. Values approaching 100% are considered the most unfavourable from the perspective of landsliding (Holec et al., 2013).

LANDSLIDE SUSCEPTIBILITY ANALYSIS AND RESULTS

REPRESENTATION OF LANDSLIDES WITHIN INDIVIDUAL PARAMETRIC MAPS

Analysing the representation of landslides within the individual parametric map classes provides key insights into the factors influencing their formation and distribution. For each parameter, a table is provided showing the distribution of individual classes in km^2 and percentages. In the case of elevation, aspect, slope, and curvature, the tables show separate values for both the DEM 5.0 and DEM 3.5 models.

Table 8

Distribution of engineering-geological classes within the landslide-affected area (km² and %)

Class	Genetical type	Landslide [km²]	Landslide [%]
1	Slope deposits	26.65	60.32
2	Fluvial deposits	0.02	0.06
3	Aeolian deposits	0.63	1.44
4	Neogene strata	6.11	13.83
5	Proluvial deposits	<0.01	<0.01
6	Neovolcanic rocks	10.77	24.37

From a lithological perspective, the overwhelming majority of landslides are concentrated within slope (deluvial) deposits. These are primarily composed of loams and sandy loams, but also include stony-loamy deposits, debris-clay deposits, and sandy-loamy gravels with rock fragments. The high concentration of landslides in these units is attributed to their unconsolidated nature and high permeability. This heterogeneous mixture is highly susceptible to rapid saturation during heavy rainfall, which increases pore water pressure and significantly reduces the shear strength of the material.

Furthermore, a significant portion of failures is linked to the contact between the volcanic bedrock (neovolcanic rocks) and the underlying Neogene strata. In this geological setting, the rigid andesites and their volcanoclastic equivalents commonly overlie the plastic clays and silts of the Stretava Formation (and Košice gravels). This lithological interface, which also contains sands and tuffaceous horizons, acts as an impermeable sliding base. Groundwater accumulating at this boundary creates ideal conditions for the development of failure surfaces, leading to the high landslide density observed at the transition between the mountains and the basin. The complete distribution of landslides across all engineering-geological units is detailed in Table 8.

Regarding land cover, the highest landslide density is observed in forest stands and arable land. The high representation in forested areas is typical of the steeper, higher-elevation zones of the Slanské vrchy Mts., where ancient landslides are commonly stabilized by vegetation but remain a dominant part of the geomorphological record. The significant occurrence on arable land, however, points to the influence of human activity; intensive agricultural use on the foothills can disrupt slope equilibrium and alter natural drainage patterns, especially on sensitive Neogene substrates. These findings are summarized in Table 9.

The analysis of elevation reveals a clear landslide “hotspot” in the 212–312 m a.s.l. range for both the DEM 5.0 and DEM 3.5 models. This altitudinal belt corresponds to the transitional zone between the volcanic mountain range and the sedimentary basin. This zone is characterized by a critical combination of increased slope gradients and the presence of landslide-prone Neogene strata at the surface. As elevation increases above 512 m a.s.l., the landslide frequency drops significantly, as these higher areas are dominated by more competent, massive volcanic units with higher internal stability. Detailed area and percentage shares for each elevation class are shown in Table 10.

Table 9

Distribution of land cover classes within the landslide-affected area (km² and %)

Class	Description	Landslide [km²]	Landslide [%]
1	Transport infrastructure	0.18	0.40
2	Built-up area	0.36	0.83
3	Meadows	1.48	3.34
4	Arable land	15.46	35.00
5	Shrubland	2.28	5.17
6	Forests	22.05	49.90
7	Gardens	2.34	5.29
8	Water bodies	0.04	0.08

Despite the significant differences in the resolution of the two models, the distribution of landslides across elevation classes for both DEM 5.0 and DEM 3.5 is remarkably similar. The percentage values for individual intervals differ only minimally. This suggests that the overall altitudinal distribution of landslides is not fundamentally influenced by the differing levels of detail present in the two digital elevation models. This finding corroborates that the main altitudinal belts prone to landslide development remain consistent regardless of the underlying DEM used.

The distribution of landslides based on slope aspect reveals significant spatial patterns that point to the influence of local meteorological and microclimatic conditions. Instead of a dispersed distribution, a clear concentration of landslide-affected areas is observable along specific orientations.

A direct comparison of both digital elevation models reveals a consistent trend: the highest concentration of landslides is situated on west-facing slopes, followed by northwestern and northeastern aspects. This higher frequency on windward slopes (W, NW) is likely linked to the prevailing wind directions in the Slanské vrchy Mts., which bring the majority of precipitation-bearing fronts. These slopes are exposed to higher cumulative rainfall, leading to more frequent saturation of the deluvial cover and the underlying Neogene clays. In contrast, the lower proportion of landslides on south- and south-east-facing slopes may be attributed to higher solar radiation and increased evapotranspiration, which help maintain lower soil moisture levels.

It is important to emphasize that these results represent the spatial frequency and concentration of existing landslides within specific classes, rather than a final susceptibility assessment. The consistency between the DEM 5.0 and DEM 3.5 models confirms that the directional influence on landslide occurrence is a robust geographical feature of the area, although the lower-resolution model tends to slightly over-represent the area

Table 10

Distribution of elevation classes within the landslide-affected area (km² and %)

Class	Interval [m a.s.l.]	Landslide DEM 5.0 [km²]	Landslide DEM 5.0 [%]	Landslide DEM 3.5 [km²]	Landslide DEM 3.5 [%]
1	(<212)	3.08	6.98	3.04	6.89
2	(212–312)	19.76	44.72	19.92	45.07
3	(312–412)	10.63	24.05	10.54	23.86
4	(412512)	6.22	14.07	6.17	13.97
5	(512–612)	3.22	7.29	3.21	7.27
6	(612–712)	1.07	2.42	1.08	2.45
7	(712–812)	0.21	0.47	0.22	0.49
8	(>812)	0.00	0.00	0.00	0.00

Table 11

Distribution of aspect classes within the landslide-affected area (km² and %)

Class	Interval [°]	Landslide DEM 5.0 [km²]	Landslide DEM 5.0 [%]	Landslide DEM 3.5 [km²]	Landslide DEM 3.5 [%]
1	flat (–1)	0.04	0.09	0.02	0.05
2	N (337.5–22.5)	5.34	12.08	5.24	11.87
3	NE (22.5–67.5)	5.91	13.37	6.44	14.57
4	E (67.5–112.5)	4.94	11.17	4.99	11.30
5	SE (112.5–157.5)	4.19	9.49	4.01	9.07
6	S (157.5–202.5)	4.06	9.18	3.63	8.23
7	SW (202.5–247.5)	5.88	13.32	5.28	11.94
8	W (247.5–292.5)	8.05	18.22	8.60	19.47
9	NW (292.5–337.5)	5.78	13.08	5.97	13.52

Table 12

Distribution of slope classes within the landslide-affected area (km² and %)

Class	Interval [°]	Landslide DEM 5.0 [km²]	Landslide DEM 5.0 [%]	Landslide DEM 3.5 [km²]	Landslide DEM 3.5 [%]
1	(<2)	1.59	3.61	0.57	1.24
2	(2–3)	2.08	4.72	1.26	2.82
3	(3–5)	7.96	18.01	8.47	19.23
4	(5–7)	9.66	21.87	12.17	28.10
5	(7–11)	12.02	27.21	14.21	32.10
6	(11–17)	6.54	14.81	5.90	13.07
7	(17–20)	1.43	3.23	0.80	1.73
8	(20–31)	2.25	5.09	0.76	1.63
9	(>31)	0.64	1.46	0.04	0.07

Table 13

Distribution of curvature classes within the landslide-affected area (km² and %)

Class	Interval [m⁻¹]	Landslide DEM 5.0 [km²]	Landslide DEM 5.0 [%]	Landslide DEM 3.5 [km²]	Landslide DEM 3.5 [%]
1	Convex (< –0.00025)	21.80	49.33	16.52	37.38
2	Linear (–0.00025–0.00025)	0.90	2.03	14.84	33.58
3	Concave (>0.00025)	21.49	48.64	12.83	29.03

of western aspects due to its inherent smoothing effect. The detailed statistical shares for all aspect classes are summarized in Table 11.

Slope gradient is one of the most critical factors for slope stability as it directly governs the distribution of gravitational forces. An increase in slope angle leads to a higher shear stress acting along potential failure surfaces, while simultaneously decreasing the normal stress component that contributes to frictional resistance. In the context of the Slanské vrchy Mts., identifying the critical slope thresholds is essential for understanding where the balance between driving and resisting forces is most frequently disturbed.

The analysis of landslide distribution across slope classes reveals that the highest concentration of deformation structures in both models occurs within the 5 to 11° range, with a peak in the 7–11° interval. This confirms that landslides in the study area are primarily tied to moderate slopes, where thick accumulations of deluvial deposits on a sensitive Neogene substrate create a high potential for failure. Detailed quantitative data for all slope classes are shown in Table 12.

A significant discrepancy between the two models arises in the steeper categories (>17°). The high-resolution DEM 5.0 identifies a much higher proportion of landslide areas in these steep intervals compared to DEM 3.5. This is due to the LiDAR-based model's ability to accurately capture the internal micro-morphology of landslides, such as steep headscarps, secondary scarps, and tension cracks. These features commonly exhibit gradients far exceeding the original slope angle.

While DEM 5.0 provides a superior representation of the present-day geomorphology, these high-gradient values represent the result of the landslide process rather than the conditions that initiated it. In contrast, DEM 3.5, due to its lower resolution and inherent smoothing effect, filters out these post-failure micro-features. This generalization results in a distribution that reflects the macro-relief rather than the specific landslide anatomy. In susceptibility modelling, this distinction is crucial, as the extreme slopes captured by high-resolution models can disproportionately influence the statistical weighting of steeper classes.

The analysis of landslide distribution across terrain curvature classes provides essential insights into the hydrological and geomorphological processes governing slope instability. Curvature directly influences the dynamics of surface runoff and the spatial concentration of soil moisture, which are primary triggers for failure in the clay-rich substrates of the Slanské vrchy Mts.

Based on the DEM 5.0 data, the landslides show a nearly equal distribution between convex and concave terrain forms, while linear (planar) forms represent only a negligible share. This balanced distribution is highly characteristic of the complex, hummocky micro-relief typical of landslide bodies. The high-resolution LiDAR data captures the intricate alternation of secondary scarps and depressions (concave forms), where water tends to converge, and accumulation lobes or transverse ridges (convex forms). This suggests that the model is capturing the internal morphological complexity of the landslide itself, rather than just the pre-failure slope.

In stark contrast, the DEM 3.5 data shows a significantly higher proportion of landslides within linear forms. This disparity is a direct result of the smoothing effect and lower resolution of the older model, which fails to detect the subtle micro-topographic features of the landslide surface. By generalizing these features into planar surfaces, the DEM 3.5 loses critical information regarding water convergence zones, which are essential for accurate susceptibility mapping. The detailed statistical distribution for all curvature classes is summarized in Table 13.

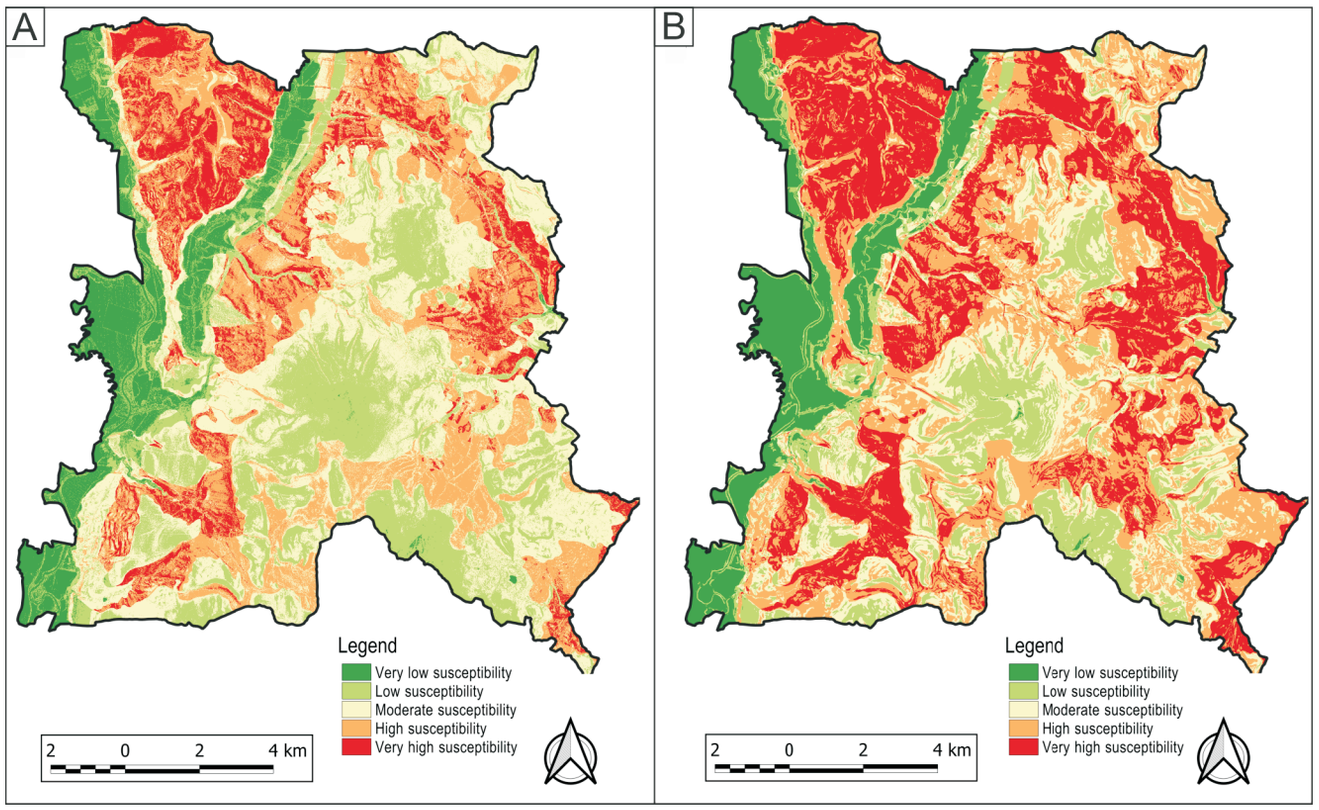

Fig. 8A – landslide susceptibility map of the study area based on DEM 5.0; B – DEM 3.5 results of the frequency ratio (processed in QGIS)

Table 14

Distribution of landslide susceptibility classes based on frequency ratio analysis using DEM 5.0 within the entire study area and landslide-affected area (km² and %)

Class	Description	Area [km²]	Area [%]	Area landslide [km²]	Area landslide [%]
1	Very low susceptibility	19.15	10.10	0.04	0.08
2	Low susceptibility	44.81	23.63	3.77	8.53
3	Moderate susceptibility	57.96	30.57	12.82	29.01
4	High susceptibility	46.33	24.44	17.34	39.25
5	Very high susceptibility	21.35	11.26	10.22	23.13

RESULTS

This study utilized three distinct statistical methods frequency ratio, bivariate analysis, and multivariate analysis to assess landslide susceptibility. Given that each method was applied to two separate datasets derived from DEM 5.0 and DEM 3.5, a total of six landslide susceptibility maps were generated. The performance of each map was evaluated using a Receiver Operating Characteristic (ROC) curve, which will be shown along with a detailed table for each method.

For all six of the final susceptibility maps, the continuous intensity values were reclassified into five distinct classes: very low, low, moderate, high, and very high. Initially, we attempted to use the "natural breaks" method for reclassification, but the results were unsatisfactory, as a significant portion of the landslide-affected area was incorrectly categorized into the lowest susceptibility class. Therefore, this reclassification was performed using the Geometrical Interval method. The following sections provide a detailed overview of the results for each analytical approach, including the susceptibility maps, comprehensive tables that show the distribution of these classes across both the entire study area and specifically within the landslide-affected zones, and the corresponding ROC curves that illustrate the predictive performance of each model.

Frequency ratio analysis of the DEM 5.0 data shows that the 'High susceptibility' class covers the largest portion of the study area (24.44%; Fig. 8A). The 'Very high susceptibility' class, which covers 11.26% of the study area, contains 23.13% of all mapped landslides. The 'High susceptibility' class contains an even larger portion, with 39.25% of landslides found within its boundaries. Together, these two classes contain a combined 62.38% of the total landslide area. Conversely, the 'Very low susceptibility' class, covering 10.10% of the study area, contains only a negligible 0.08% of landslides (Table 14).

The DEM 3.5 data shows a different distribution (Fig. 8B). The 'High susceptibility' class covers the largest portion of the study area (30.19%), with the 'Very high susceptibility' class covering a substantial 25.75%. This model demonstrates even greater predictive power. The 'Very high susceptibility' class accounts for a remarkable 50.48% of all mapped landslides, while the 'High susceptibility' class contains an additional 35.38% of the landslides. In total, these two classes constitute 85.86% of

Table 15

Distribution of landslide susceptibility classes based on frequency ratio analysis using DEM 3.5 within the entire study area and landslide-affected area (km² and %)

Class	Description	Area [km²]	Area [%]	Area landslide [km²]	Area landslide [%]
1	Very low susceptibility	19.92	10.51	0.02	0.04
2	Low susceptibility	27.23	14.36	1.61	3.64
3	Moderate susceptibility	36.39	19.19	4.62	10.45
4	High susceptibility	57.24	30.19	15.63	35.38
5	Very high susceptibility	48.82	25.75	22.30	50.48

the landslide area. The 'Very low susceptibility' class, covering 10.51% of the study area, contains only a minimal 0.04% of landslides (Table 15).

The predictive performance of the Frequency Ratio models was validated using Receiver Operating Characteristic (ROC) curves. The model based on DEM 3.5 achieved an Area Under the Curve (AUC) value of 76.18%, indicating a high level of accuracy. In comparison, the model using DEM 5.0 showed a slightly lower predictive performance, with an AUC value of 74.58%. The results demonstrate that the model derived from the DEM 3.5 was more effective at concentrating the observed landslides into the highest susceptibility classes (Fig. 9).

For the Bivariate Analysis using DEM 5.0, the 'Very high susceptibility' class covers a significant portion of the study area (21.22%; Fig. 10A). More importantly, this class contains the largest share of landslides, accounting for 38.30% of the total landslide area. The 'High susceptibility' class, which covers 19.19% of the study area, contains an additional 30.87% of the landslides. Cumulatively, the two highest classes account for 69.17% of the total landslide area. In contrast, the 'Very low susceptibility' class, despite covering 14.13% of the area, contains a negligible 0% of the landslides, highlighting the model's effectiveness at identifying stable areas (Table 16).

The Bivariate Analysis of the DEM 3.5 data shows a very similar distribution (Fig. 10B). The 'Very high susceptibility' class, covering 19.78% of the study area, captures 38.34% of all mapped landslides. The 'High susceptibility' class accounts for an additional 31.02% of landslides, while covering 20.05% of the study area. Together, these two classes concentrate a cumulative 69.36% of the total landslide area, a result almost identical to the DEM 5.0 model. The 'Very low susceptibility' class (13.72% of the study area) also contains a minimal 0.01% of the observed landslides (Table 17).

The predictive performance of the Bivariate Analysis models was again validated using ROC curves. The model based on DEM 3.5 achieved an AUC value of 75.77%, indicating a high level of accuracy. In comparison, the model using DEM 5.0 showed a slightly lower predictive performance, with an AUC

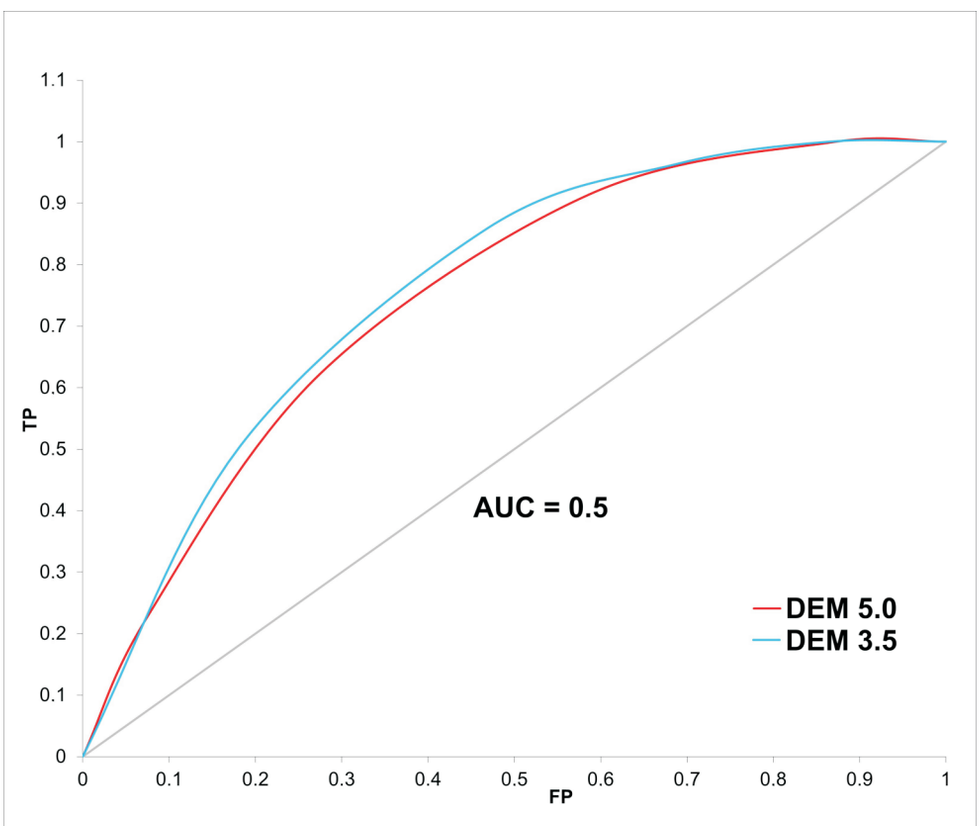

Fig. 9. ROC curves for Frequency ratio

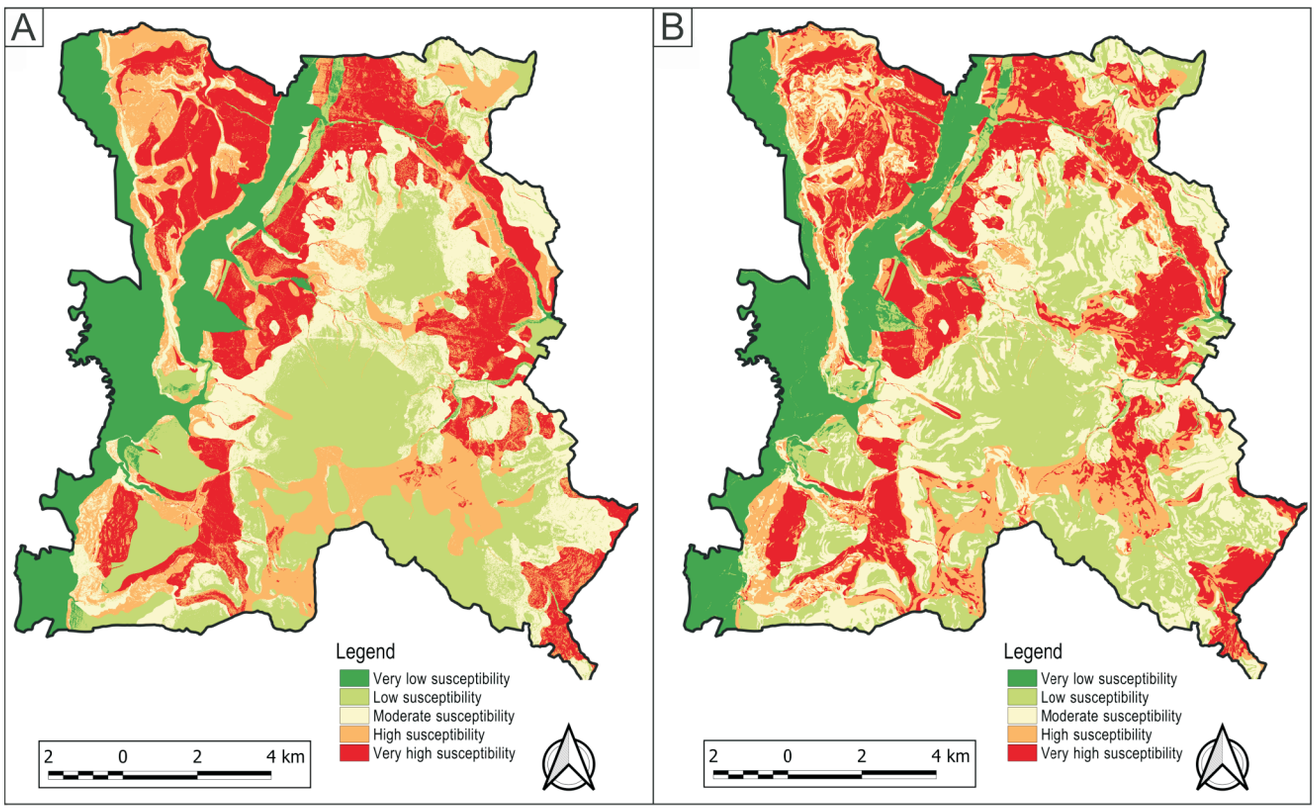

Fig. 10A – landslide susceptibility map of study area based on DEM 5.0; B – DEM 3.5 results of bivariate analysis (processed in QGIS)

Table 16

Distribution of landslide susceptibility classes based on bivariate analysis using DEM 5.0 within the entire study area and landslide-affected area (km² and %)

Class	Description	Area [km²]	Area [%]	Area landslide [km²]	Area landslide [%]
1	Very low susceptibility	26.79	14.13	0.00	0.00
2	Low susceptibility	48.40	25.52	5.40	12.23
3	Moderate susceptibility	37.81	19.94	8.21	18.60
4	High susceptibility	36.38	19.19	13.63	30.87
5	Very high susceptibility	40.23	21.22	16.92	38.30

Table 17

Distribution of landslide susceptibility classes based on bivariate analysis using DEM 3.5 within the entire study area and landslide-affected area (km² and %)

Class	Description	Area [km²]	Area [%]	Area landslide [km²]	Area landslide [%]
1	Very low susceptibility	26.01	13.72	0.00	0.01
2	Low susceptibility	44.75	23.60	4.09	9.26
3	Moderate susceptibility	43.34	22.86	9.45	21.38
4	High susceptibility	38.01	20.05	13.71	31.02
5	Very high susceptibility	37.51	19.78	16.94	38.34

value of 74.33%. This result is consistent with the Frequency Ratio findings, showing that the model derived from the DEM 3.5 was more effective at concentrating the observed landslides into the highest susceptibility classes (Fig. 11).

The results from the multivariate analysis using DEM 5.0 data shows 29,749 different unique combinations, of which 921 reached a 100% probability of slope deformation occurrence. As an example, we can mention the unique conditional unit (UCU) labeled as combination 1 3 1 1 2 4. In this case, it refers to slope deposits, an elevation between 312 and 412 m a.s.l., a slope of 0-2 degrees, flat terrain, linear terrain curvature, and arable land. The first ten most unfavorable combinations out of the total number are listed in Table 18.

Using multivariate analysis of the DEM 5.0 data, the 'Moderate susceptibility' class covers the largest portion of the study area (27.06%; Fig. 12A). From a validation standpoint, the 'Very high susceptibility' class, which covers 9.47% of the total area, accounts for 25.83% of all mapped landslides. The 'High susceptibility' class contains a significant portion of the observed landslides, with 45.16% of the landslide area. Together, the two

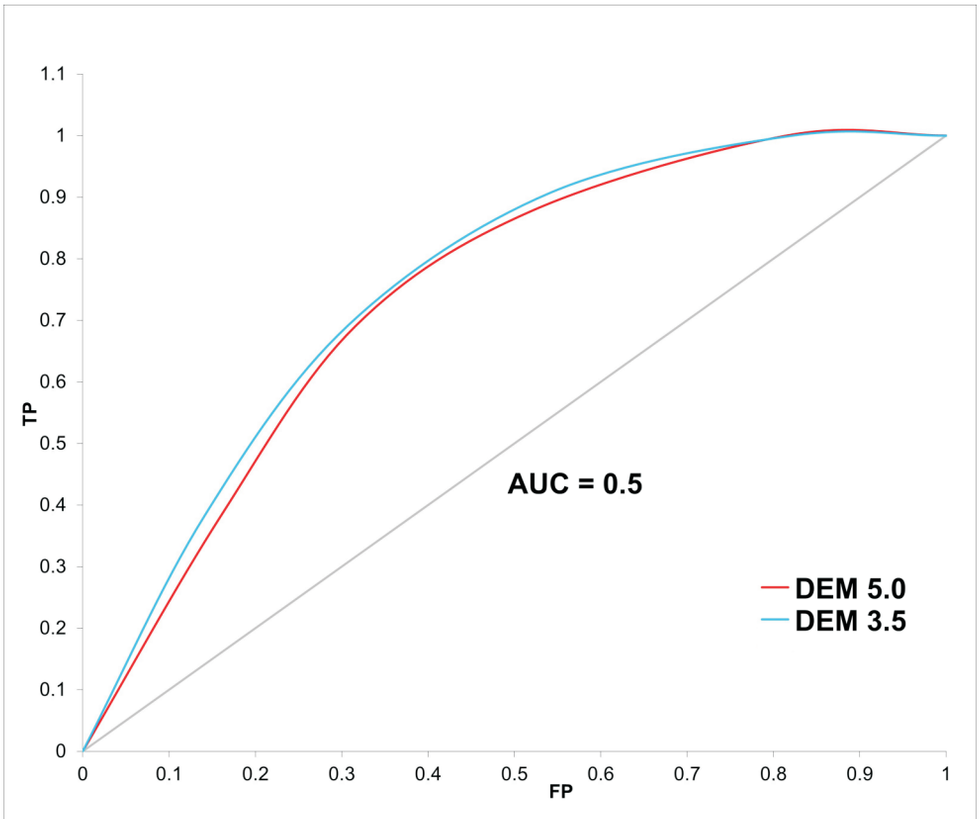

Fig. 11. ROC curves for Bivariate analysis

Table 18

First ten most unfavourable combinations from multivariate analysis using the DEM 5.0 data

Order	UCU	Lithology	Elevation	Slope	Aspect	Curvature	Land cover	Area [m²]	Landslide layer overlay [%]
1	131124	1	3	1	1	2	4	1543	100
2	155333	1	5	5	3	3	3	798	100
3	655434	6	5	5	4	3	4	635	100
4	655414	6	5	5	4	1	4	606	100
5	655514	6	5	5	5	1	4	591	100
6	131123	1	3	1	1	2	3	582	100
7	655534	6	5	5	5	3	4	563	100
8	121126	1	2	1	1	2	6	412	100
9	641116	6	4	1	1	1	6	351	100
10	656434	6	5	6	4	3	4	327	100

highest susceptibility classes account for 70.99% of the total landslide area. In contrast, the 'Very low susceptibility' class, despite covering 23.30% of the study area, contains only 0.72% of the landslides (Table 19).

The results from the multivariate analysis using DEM 3.5 shows 16,366 different unique combinations, of which 594 reached a 100% probability of slope deformation occurrence. As an example, we can mention the unique conditional unit (UCU) labeled as combination 1 4 5 5 3 4. In this case, it refers to slope deposits, an elevation between 412 and 512 m a.s.l., a slope of 7–11°, a south-east-facing aspect, concave terrain curvature, and arable land. The first ten most unfavorable combinations out of the total number are listed in Table 20.

The multivariate analysis of the DEM 3.5 data shows a notably different distribution (Fig. 12B). The 'High susceptibility' class covers 26.98% of the study area, a proportion very similar to that from DEM 5.0. However, the 'Very high susceptibility' class, covering 17.10% of the study area, accounts for a remarkable 45.55% of all mapped landslides. The 'High susceptibility' class contains an additional 38.61% of landslides. In total, these two classes concentrate a cumulative 84.16% of the landslide area. The 'Very low susceptibility' class for this model, covering 26.96% of the study area, contains a minimal 0.41% of landslides (Table 21).

The final evaluation of the multivariate models predictive performance, as shown by their Receiver Operating Characteristic (ROC) curves, corroborates the consistent trend seen across all methods. The DEM 5.0 model achieved a high Area Under the Curve (AUC) value of 80.89%. However, the DEM 3.5 model once again outperformed it, with a higher AUC value of 84.18% (Fig. 13).

Across all three analytical methods – frequency ratio, bivariate analysis, and multivariate analysis – a consistent trend emerged. In each case, the DEM 3.5-based models demonstrated superior predictive power over their DEM 5.0 counterparts. The multivariate analysis produced the most accurate re-

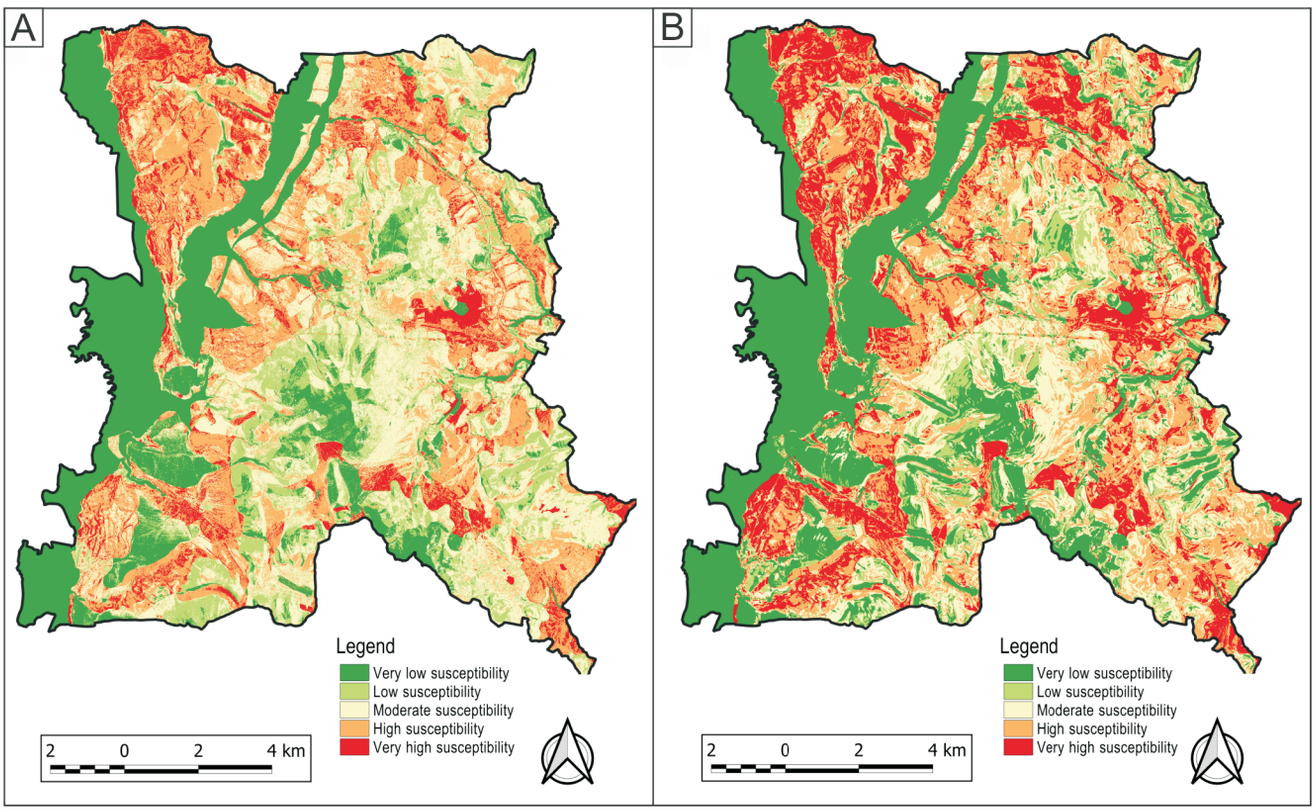

Fig. 12A – landslide susceptibility map of the study area based on DEM 5.0; B – DEM 3.5 the results of multivariate analysis (processed in QGIS)

Table 19

Distribution of landslide susceptibility classes based on multivariate analysis using DEM 5.0 within the entire study area and landslide-affected area (km² and %)

Class	Description	Area [km²]	Area [%]	Area landslide [km²]	Area landslide [%]
1	Very low susceptibility	44.19	23.30	0.32	0.72
2	Low susceptibility	25.62	13.51	2.27	5.13
3	Moderate susceptibility	51.31	27.06	10.24	23.16
4	High susceptibility	50.53	26.65	19.95	45.16
5	Very high susceptibility	17.96	9.47	11.41	25.83

Table 20

First ten most unfavorable combinations from multivariate analysis using DEM 3.5 data

Order	UCU	Lithology	Elevation	Slope	Aspect	Curvature	Land cover	Area [m²]	Landslide layer overlay [%]
1	145534	1	4	5	5	3	4	7921	100
2	134522	1	3	4	5	2	2	7600	100
3	155434	1	5	5	4	3	4	6714	100
4	644623	6	4	4	6	2	3	6579	100
5	425227	4	2	5	2	2	7	6469	100
6	645413	6	4	5	4	1	3	6319	100
7	134613	1	3	4	6	1	3	6208	100
8	136835	1	3	6	8	3	5	5940	100
9	144524	1	4	4	5	2	4	5532	100
10	646128	6	4	6	1	2	8	5370	100

Table 21

Distribution of landslide susceptibility classes based on multivariate analysis using DEM 3.5 within the entire study area and landslide-affected area (km2 and %)

Class	Description	Area [km²]	Area [%]	Area landslide [km²]	Area landslide [%]
1	Very low susceptibility	51.13	26.96	0.18	0.41
2	Low susceptibility	17.96	9.47	1.06	2.40
3	Moderate susceptibility	36.93	19.48	5.76	13.03
4	High susceptibility	51.16	26.98	17.06	38.61
5	Very high susceptibility	32.43	17.10	20.13	45.55

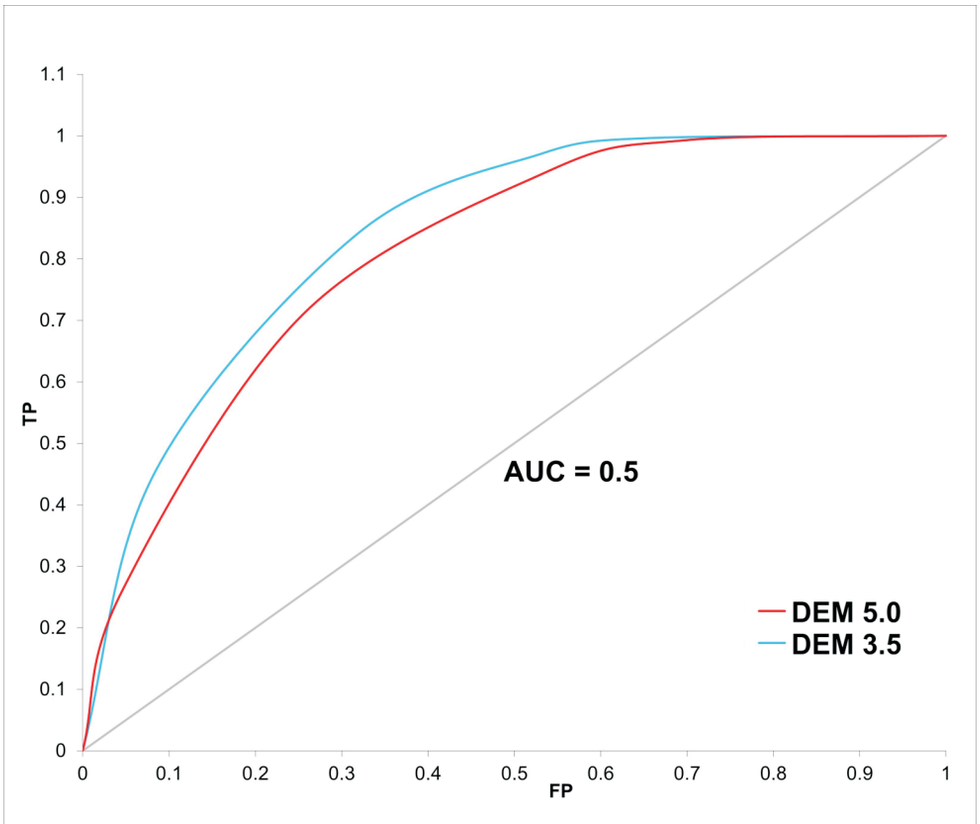

Fig. 13. ROC curves for multivariate analysis

sults for both DEMs, indicating that the use of multiple influencing factors simultaneously significantly improves the overall predictive capability. Nevertheless, the consistent outperformance of the DEM 3.5 models across the board confirms that for the purpose of landslide susceptibility mapping in this region, the older, less detailed DEM is a more effective input due to its inherent smoothing of post-failure terrain features.

DISCUSSION

This study successfully applied statistical methods (frequency ratio, bivariate, and multivariate analysis) to assess landslide susceptibility in the southern part of the Slanské vrchy Mts. A key contribution was the use of the fifth-generation digital elevation model (DEM 5.0) with a high resolution of 1 1 m. Both models demonstrated a high capability to identify areas susceptible to slope deformation, which was corroborated by high AUC values and, in particular, a high concentration of existing landslides within the two highest susceptibility classes.

However, a key finding of our work is the demonstration of the significant influence of digital elevation model resolution on the results. In every method used, the older, less detailed DEM 3.5 consistently outperformed the high-resolution DEM 5.0 in predictive accuracy. The reasons for this paradoxical result can be visually demonstrated by examining a specific, recently active landslide located near the village of Vyšný Čaj. This landslide, first registered in 1990 and highly active in 2010, is a shallow, translational-rotational slide that developed on slope (deluvial) clays and Neogene strata. A drone image of this landslide (Fig. 14) provides a clear visual context for the following analysis. The raw DEM 5.0, while providing a clear and precise view of the terrain after a landslide event, also captures morphological details that can skew the analysis.

The high-resolution DEM 5.0 allows for a highly detailed visual analysis of the terrain (Fig. 15). Its precise contours make it possible to accurately delineate the boundaries of existing landslides, including their main body, accumulation lobes, and even fine features like surface cracks. While this model is invaluable for detailed geomorphological mapping and making inventories, it becomes problematic for susceptibility modelling

When we derive the slope map from DEM 5.0 (Fig. 16A), its high resolution captures the extremely steep angles of the landslide's scarp face and other sharp breaks in the terrain. These steep slopes, which can exceed 31°, are a consequence of the landslide (post-failure morphology), not a condition that caused

Fig. 14. Vyšný Čaj landslide – drone image

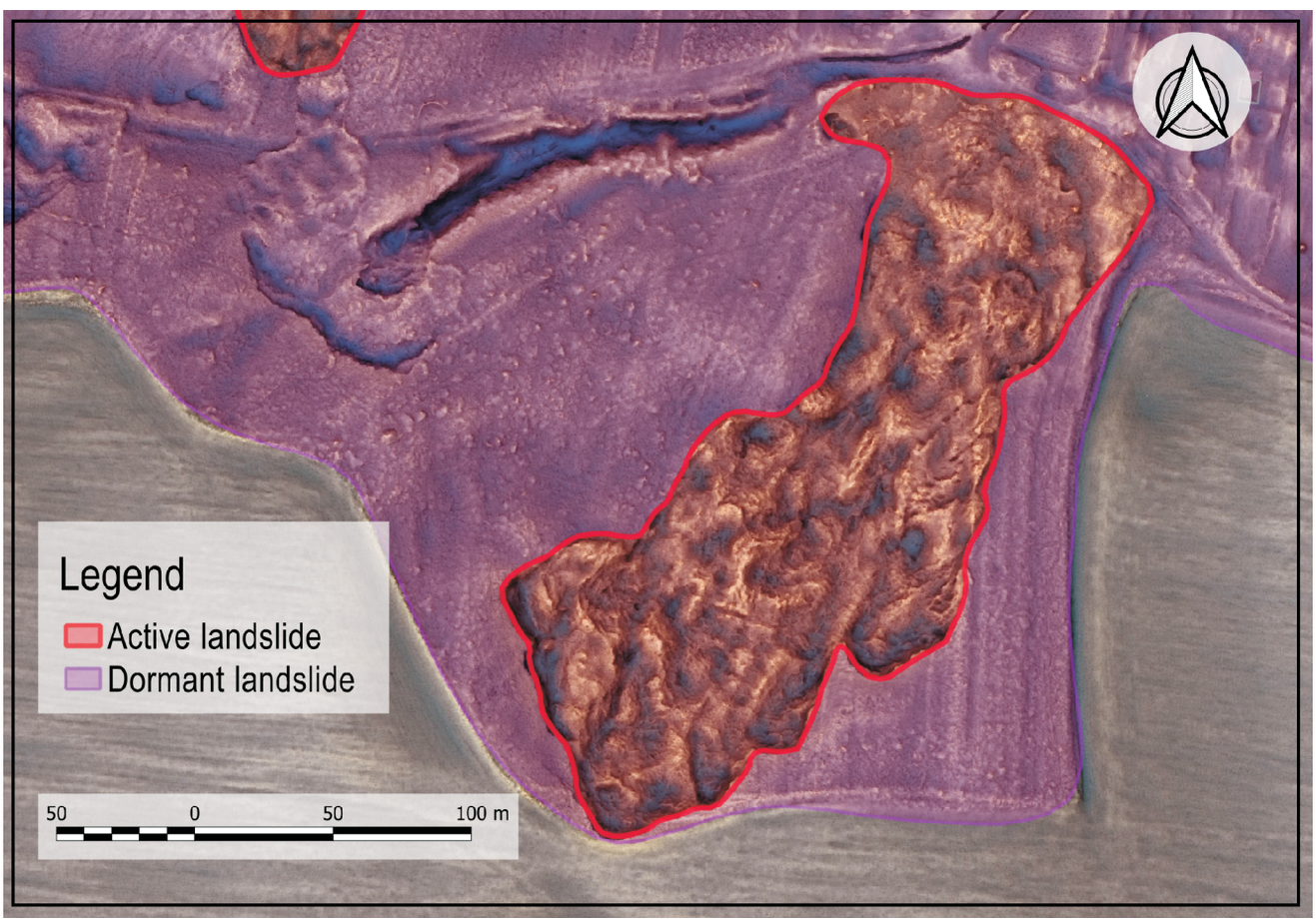

Fig. 15. Vyšný Čaj landslide – detailed DEM 5.0 visualisation of the terrain

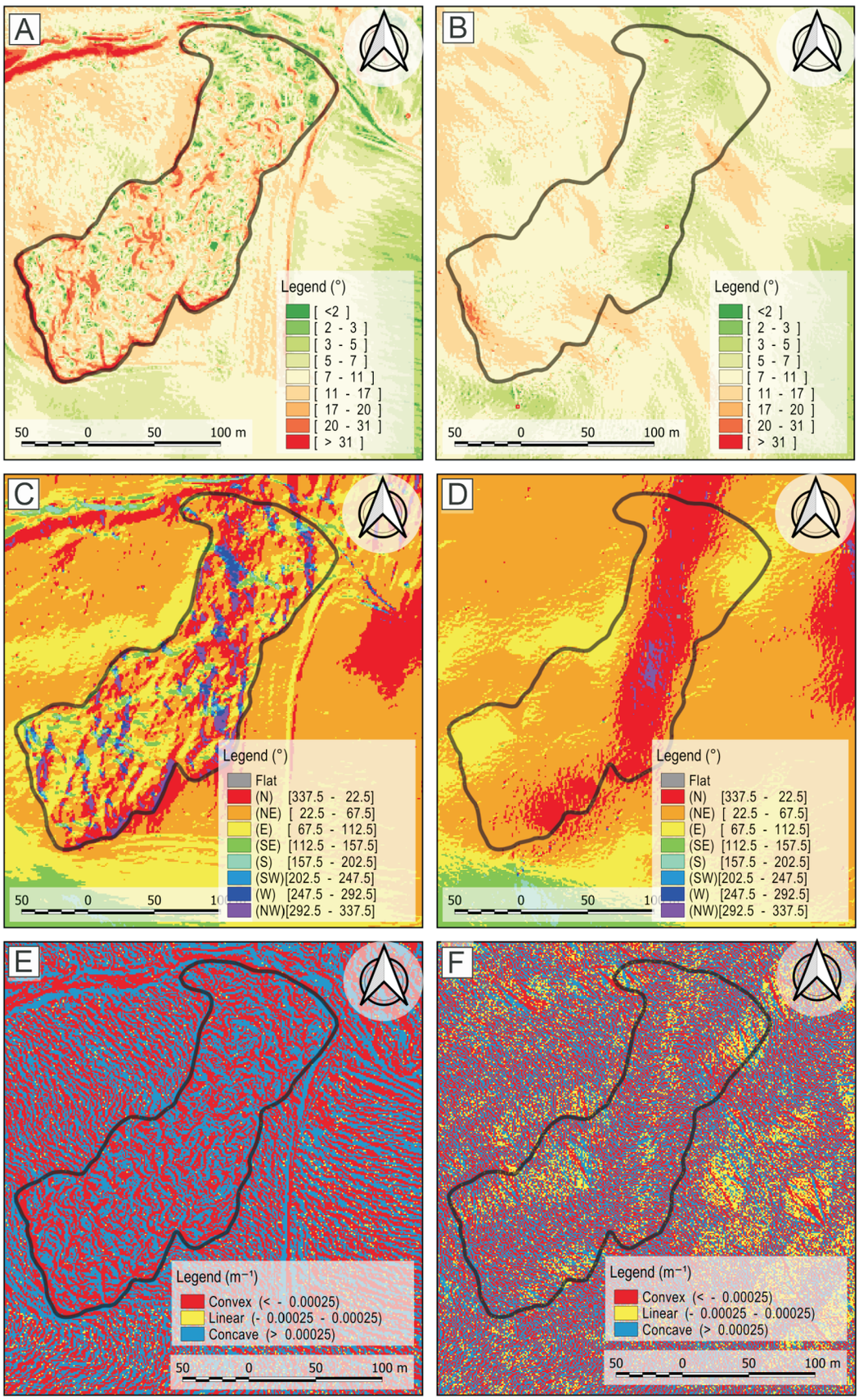

Fig. 16. Vyšný Čaj landslide – DEM 5.0 visualistation (left) for slope map (A), aspect map (C), curvature map (E) and DEM 3.5 visualisation (right) for slope map (B), aspect map (D) and curvature map (F)

it. Including these values in a susceptibility model can lead to inaccurate predictions. In stark contrast, the DEM 3.5 slope map (Fig. 16B) significantly generalizes these features due to its smoothing effect, presenting a much more uniform slope distribution that commonly obscures the true morphological complexity.

The aspect map derived from DEM 5.0 (Fig. 16C) accurately shows the main slope orientation but also captures chaotic, micro-scale variations created by small cracks, uneven surfaces, and irregular accumulations within the landslide body. These abrupt changes in aspect are largely irrelevant for predicting pre-failure conditions and introduce statistical noise. Conversely, the DEM 3.5 aspect map (Fig. 16D), with its lower resolution, provides a much smoother and generalized representation of slope orientation, effectively filtering out micro-variations but also losing fine details.

Similarly, the curvature map from DEM 5.0 (Fig. 16E) captures intricate, micro-topographic features. It records sharp convexities at the top of the scarp and pronounced concavities in the accumulation area, along with a complex mix of forms in between. While a susceptibility model should ideally identify broad convex areas of initiation and concave areas of accumulation, the high-resolution data's fine-scale features obscure the statistical signal of the pre-failure terrain. The DEM 3.5 curvature map (Fig. 16F), in turn, generalizes these features, showing a much broader distribution of linear forms due to its inherent smoothing, thereby losing critical information on water convergence/divergence at a micro-scale.

The analysis of landslide distribution across individual parameters confirmed the significance of known predisposing factors. Geological conditions exert the most significant influence, with a dominant concentration of landslides in slope and Neogene strata (>74% of the landslide area combined) underscoring their susceptibility to destabilization, especially in contact zones with volcanic rocks. Slope angle is also critical, with the highest incidence of landslides on slopes inclined at 3–11°, which is typical for translational and rotational landslides in this geological environment. The distribution of landslides by elevation and land cover reflects the spatial arrangement of geological units and human activities in the study area.

This finding underscores a critical point: when selecting input data for landslide susceptibility models, higher resolution is not always the best choice. It is more important to choose a dataset that accurately represents the environmental conditions preceding a landslide, which, in this case, is paradoxically provided by the older, less precise DEM. It is important to note that the static statistical models used are based on the analysis of predisposing factors and do not explicitly include dynamic triggering mechanisms such as intense rainfall. Future research could focus on integrating hydrological, hydrogeological data and more detailed engineering-geological information for a more comprehensive assessment of landslide susceptibility with a temporal dimension.

CONCLUSIONS

This study successfully applied three statistical methods frequency ratio, bivariate analysis, and multivariate analysis to assess landslide susceptibility in the southern part of the Slanské vrchy Mts. The models demonstrated strong predictive capabilities, effectively identifying and delineating landslide-prone areas.

A central finding of this research highlights the profound impact of digital elevation model (DEM) resolution on the reliability and accuracy of susceptibility modelling. Contrary to expectations, the models based on the high-resolution DEM 5.0 consistently showed lower predictive accuracy (as shown by lower AUC values) compared to those using the older, coarser DEM 3.5. This paradox is directly linked to the DEM 5.0's ability to capture micro-topographic features such as landslide scarps, accumulation lobes, and surface cracks that are a result of slope failure, not a cause. By smoothing out these post-failure features, the DEM 3.5 ironically provided a more realistic representation of the terrain's pre-failure conditions, leading to more accurate susceptibility maps.

It is important to note, however, that this "accuracy paradox" is particularly relevant at the detailed scale of active or recent landslides. In the case of much larger, older landslides, even the DEM 3.5 may capture the "post-failure" state, as reflected in historical contour lines. For the purpose of future modelling with high-resolution DEMs, a potential solution could be the reconstruction of the terrain "pre-landslide" by removing the landslide-affected areas from the DEM 5.0 and interpolating the surface. In this regard, a promising avenue for future research is the development of AI tools specifically designed for this purpose, capable of automating the process of terrain reconstruction for susceptibility analysis.

The resulting landslide susceptibility maps, particularly those derived from the DEM 3.5, serve as an invaluable tool for enhancing land-use planning and implementing preventive measures. They offer a highly detailed and practical overview of landslide susceptibility, making them applicable in various contexts. However, it is crucial to emphasize that these maps do not, under any circumstances, supersede the necessity for thorough, site-specific engineering-geological surveys. This distinction is paramount for ensuring responsible application of the maps in decision-making processes and for mitigating potential legal liabilities.

In conclusion, this work not only provides a sophisticated assessment of landslide susceptibility in the Slanské vrchy, but it also offers a critical insight into the complex relationship between data resolution and model performance in geohazard research. The study demonstrates that for certain applications, such as landslide susceptibility modelling, the goal is not merely to use the highest resolution data available, but to select data that best represents the relevant predisposing factors of the phenomenon being studied.

Acknowledgements. The contribution was made thanks to the financial support of the geological task 06 18 "Identification, inventory and engineering geological mapping of slope deformations", which was prepared based on the call OPKZP-PO3-SC312-2017-37 of the Operational Programme Quality of the Environment and the task was implemented in accordance with its Priority Axis 3: "Support for risk management, emergency management and resilience to emergency events affected by climate change", investment priority 3.1 "Support for investments to address specific risks, ensure disaster prevention and develop disaster management systems", specific objective 3.1.2: "Increasing the effectiveness of preventive and adaptation measures to eliminate environmental risks (except flood prevention measures)".

REFERENCES

Ahmed, M., Titti, G., Trevisani, S., Borgatti, L., Francioni, M., 2025. Is higher resolution always better? A comparison of open-access DEMs for optimized slope unit delineation and regional landslide, prediction. Natural Hazards and Earth System Sciences, **25**: 2519–2539; https://doi.org/10.5194/nhess-25-2519-2025

Bednarik, M., 2007. Assessment of landslide risk for the requirement of spatial planning documentation (in Slovak). Ph.D. thessis, Comenius University, Faculty of Natural Sciences, Bratislava.

Bednarik, M., Pauditš, P., 2010. Different ways of landslide geometry interpretation in a process of statistical landslide susceptibility and hazard assessment: Horná Súča (Western Slovakia) case study. Environmental Earth Sciences, **61**: 733–739; https://doi.org/10.1007/s12665-009-0387-8

Bednarik, M., Šimeková, J., Žec, B., Grman, D., Boszáková, M., 2014a. A Large-Scale Landslide Hazard Assessment within the Flysch Formation in the Slovak Republic. Slovak Geological Magazine, **14**: 65–78.

Bednarik, M., Pauditš, P., Ondrášik, R., 2014b. Various techniques for evaluating landslide hazard maps reliability: bivariate vs. multivariate statistical model (in Slovak with English summary). Acta Geologica Slovaca, **6**: 71–84.

Brabb, E.E., 1984. Innovative approaches to landslide hazard mapping. Proceedings of 4th International Symposium on Landslides, **1**, 307–324.

Buša, J., Tornyai, R., Bednarik, M., Greif, V., Rusnák, M., 2019. Landslide hazard assessment using bivariate and multivariate statistical analysis in Košická kotlina basin (Western Carpathians) (in Slovak with English summary). Geografický časopis, **71**: 383–405.

Carrara, A., 1983. A Multivariate Model for Landslide Hazard Evaluation. Journal of the International Association for Mathematical Geology, **15**: 403–426; https://doi.org/10.1007/BF01031290

Chung, C.F., Fabbri, A.G., 1999. Probabilistic prediction models for landslide hazard mapping. Photogrammetric Engineering and Remote Sensing, **65**: 1389–1399.

DEM 3.5, 2013. Digital elevation model. Geodesy and Cartography Institute, Bratislava.

Grman, D., Boszaková, M., Magdošová, M., Ondrejka, J., Potančok, L., Syčevová, M., Takáč, P., Udič, P., Dvořák, M., Ádámová, M., 2010. Inžinierskogeologický prieskum havarijných zosuvov v Košickom kraji (in Slovak). MŽP SR, Bratislava, GEO Slovakia, s.r.o., Košice. Manuscript – Geofond, Bratislava.

Grman, D., Boszáková, M., Hajduková, J., Magdošková, M., Syčev, V., Takáč, P., Udič, M., Wanieková, D., Stercz, M., Žec, B., Žurbej, J., Balážová, R., Bednarik, M., Laho, M., Liščák, P., Páleník, M., Páleník, M., Smolka, J., Smolka, M., Sluka, V., Šimeková, J., Farkašovský, R., Jacko, S., Janočko, J., 2011. Inžinierskogeologické mapovanie svahových deformácií v najohrozenejších územiach flyšového pásma v M 1:10 000 (in Slovak). GEO Slovakia, s.r.o., Košice.

Guimpier, A., Conway, S.J., Pajola, M., Lucchetti, A., Simioni, E., Re, C., Noblet, A., Mangold, N., Thomas, N., Cremonese, G., 2022. Pre-landslide topographic reconstruction in Baetis Chaos, Mars using a CaSSIS Digital Elevation Model. Planetary and Space Science, **218**, 105505; https://doi.org/10.1016/j.pss.2022.105505

Gulbet, E., Getahun, B., 2024. Landslide susceptibility mapping using frequency ratio and analytical hierarchy process method in Awabel Woreda, Ethiopia. Quaternary Science Advances, **16**, 100246; https://doi.org/10.1016/j.qsa.2024.100246

Guzzetti, F., Carrara, A., Cardinali, M., Reichenbach, P., 1999. Landslide hazard evaluation: a review of current techniques and their application in a multi-scale study, Central Italy. Geomorphology, **31**: 181–216; https://doi.org/10.1016/S0169-555X(99)00078-1

Guzzetti, F., Reichenbach, P., Cardinali, M., Galli, M., Ardizzone, F., 2005. Landslide hazard assessment in the Staffora Basin, Northern Italian Apennines. Geomorphology, **72**: 272–299; https://doi.org/10.1016/j.geomorph.2005.06.002

Holec, J., Bednarik, M., Šabo, M., Minár, J., Yilmaz, I., Marschalko, M., 2013. A small scale landslide susceptibility assessment for the territory of Western Carpathians. Natural Hazards, **6**: 1081–1107; https://doi.org/10.1007/s11069-013-0751-6

Holec, J., Bednarik, M., Liščák, P., Žilka, A., Vitovič, L., 2018. Assessment of debris flow susceptibility using bivariate and multivariate statistical analyses and verification based on catastrophic events from 2014 in the Krivánska Fatra Mountains, Slovakia. Acta Geologica Slovaca, **10**: 1–19.

Hungr, O., Leroueil, S., Picarelli, L., 2014. The Varnes classification of landslide types, an update. Landslides, **11**: 167–194; https://doi.org/10.1007/s10346-013-0436-y

Jurko, J., 2003. Map of landslides susceptibility in the Liptovská kotlina basin (in Slovak). Diploma thesis, Comenius University, Faculty of Natural Sciences, Bratislava.

Kaličiak, I.M., Žec, B., 1995. Review of Neogene volcanism of Eastern Slovakia. Vulcanologica, **7**: 87–95.

Kaličiak, M., Baňacky, V., Jacko, S., Janočko, J., Karoli, S., Petro, Ľ., Spišiak, Z., Vozar, J., Žec, B., Ivanička, J., Vass, D.,1996. Geologická mapa Slanských vrchov a Košickej kotliny – južná časť, M 1:50 000 (in Slovak). Bratislava (GS SR).

Krumpálová, M., 2008. Landslide hazard assessment in Breznianska kotlina basin (in Slovak). Diploma thesis, Comenius University, Faculty of Natural Sciences, Bratislava.

Leitmanová, K., Gálová, L., 2023. Slovakia Already Has a Digital Terrain Model of the Whole Territory (in Slovak with English summary). Geodetický a kartografický obzor, **69/111**: 265–273.

Li, L., Lan, H., 2023. Bivariate landslide susceptibility analysis: clarification, optimization, open software and preliminary comparison. Remote Sensing, **15**, 1418; https://doi.org/10.3390/rs15051418

Liščák, P., Pauditš, P., Petro, Ľ., Iglárová, Ľ., Ondrejka, P., Dananaj, I., Brček, M., Baráth, I., Vlačiky, M., Németh, Z., Záhorová, Ľ., Antalík, M., Repčiak, M., Drotár, D., 2010. Registration and evaluation of newly evolved slope failures in 2010 in Prešov and Košice regions. Mineralia Slovaca, **42**: 393–406.

Liščák, P., Pauditš, P., Petro, Ľ., Jelínek, R., Ondrejka, P., Dananaj, I., Mašlár, E., Mašlárová, I., Ondrášiková, B., Fraštia, M., 2018. Identifikácia, registrácia a inžinierskogeologické mapovanie svahových deformácií (A1). Projekt geologickej úlohy, etapa orientačný inžinierskogeologický prieskum (in Slovak). ŠGÚDŠ Bratislava.

Liščák, P,. Pauditš, P., Bystrická, G, Teták, F., Maglay, J., Dananaj, I., Ondrus, P., Mašlár, E., Mašlárová, I., Olšavský, M., Pelech, O., Vitovic, L., Leitmannová, K., Fraštia, M., Papco, J., 2022. Use of DMR 5.0 from the Airborne Laser Scanning in Solving Geological Tasks of ŠGÚDŠ (in Slovak with English summary). Geodetický a kartogracký obzor, **68/110**: 149–159; https://egako.eu/wp-content/uploads/2022/08/liscak_aj_2022_08.pdf

Magulová, B., 2009. Using GIS for creation of geohazards map as a base for landuse planning (in Slovak with English summary). Acta Geologica Slovaca, **1**: 25–32.

Matula, M., Ondrášik, R., Holzer, R., Wagner, P., Hrašna, M., Letko, V., 1983. Metódy inžinierskogeologického výskumu (in Slovak). Bratislava (Univerzita Komenského).

Mazúr, E., Lukniš, M., 1978. Regionálne geomorfologické členenie SSR (in Slovak). Geografický časopis, **30**: 101–125 + 1 map (1:1 000 000).

Mitasova, H., Mitas, L., Brown, W.M., Gerdes, D.P., Kosinovsky, I., Baker, T., 1995. Modelling spatially and temporally distributed phenomena: new methods and tools for GRASS GIS. International Journal of GIS, **9**: 433–446; https://doi.org/10.1080/02693799508902048

Nemčok, A., 1982. Zosuvy v slovenských Karpatoch (in Slovak). Veda, Bratislava.

Okoli, J., Nahazanan, H., Nahas, F., Kalantar, B., Shafri, H.Z.M., Khuzaimah, Z., 2023. High-resolution lidar-derived DEM for landslide susceptibility assessment using AHP and Fuzzy Logic in Serdang, Malaysia. Geosciences, **13,** 34; https://doi.org/10.3390/geosciences13020034

Ondrášik, M., Smolárová, H., Gluch, A., Marsina, K., Siráňová, Z., Kordík, J., Slaninka, I., Marcin, D., Malík, P., Švastva, J., Potfaj, M., Dlapa, P., Ďuriš, M., Juráni, B., Mičuda, R., Šimkovic, I., Frankovská, J., Dananaj, I., Liščák, P., Jelínek, R., Pauditš, P., Ondrejka, P., Šefčíková, B., Iglárová, Ľ., Magalová, D., Okoličányiová, K., Pristaš, J., Hók, J., 2005. Súbor regionálnych máp geologických faktorov životného prostredia regiónu Myjavská pahorkatina a Biele Karpaty (in Slovak). Záverečná správa. Bratislava (ŠGÚDŠ).

Pauditš, P., 2005. Assessment of territory susceptibility to landslides using statistical methods in GIS environment (in Slovak with English summary). Ph.D. thesis, Comenius University, Faculty of Natural Sciences, Bratislava.

Pauditš, P., 2006. Hodnotenie náchylnosti územia na zosúvanie s využitím štatistických metód v prostredí GIS (in Slovak). Geologické práce, Správy: **112**: 41–58.

Pauditš, P., Bednarik, M., 2002. Using GIS in evaluation of landslide susceptibility in Handlovska kotlina basin. Proceedings of the 1st European conference on landslide: 437–441. Lisse, Praha (Swets & Zeitlinger).

Pauditš, P., Kralovičová, L., Bednarik, M., 2014. Landslide. Hazard Assessment Using Spatial Statistical Methods. Slovak Geological Magazine, **1/2014**: 41–63.

Pourghasemi, H.R., Pradhan, B., Gokceoglu, C., 2012. Application of fuzzy logic and analytical hierarchy process (AHP) to landslide susceptibility mapping at Haraz watershed, Iran. Natural Hazards, **63**: 965–996; https://doi.org/10.1007/s11069-012-0217-2

Steger, S., 2020. The role of pre-landslide morphology in statistical modelling of landslide-prone areas. Proceedings of the Geomorphometry 2020 Conference: 190–192; https://doi.org/10.30437/GEOMORPHOMETRY2020_51

Tornyai, R., Dunčko, M., 2013. Using Bivariate and multivariate analysis to assess landslide hazard in Kysuce region (Western Carpathians) (in Slovak with English summary. Acta Geologica Slovaca, **2**: 179–193.

Tornyai, R., Koudelka, D., 2024. Utilisation of airborne laser scanning data in landslide hazard assessment – case study Čadca district, Slovakia. Acta Geologica Slovaca, **16**: 107–111.

GCCA SR, 2024. Geodesy, Cartography and Cadastre Authority of the Slovak Republic (in Slovak). Dostupné na: https://www.geoportal.sk/

Varga, M., 2006. Assessment of territory susceptibility to landslides using statistical methods in GIS environment (in Slovak with English summary). Ph.D. thesis, Faculty of Mining, Ecology, Process Control and Geotechnology, Technical University Kosice.

Varnes, D.J., 1978. Slope movement types and processes. Special Report, **176**: Landslides: Analysis and Control: 11–33. Transportation and Road Research Board, National Academy of Science, Washington.

Vlčko, J., Wagner, P., Rychlíková, Z., 1980. Evaluation of regional slope stability. Mineralia Slovaca, **12**: 275–283.